Using geophysical data to quantify stress-transmission in gap-graded granular materials

Masahide Otsubo[1], Reiko Kuwano[2], Catherine O'Sullivan[3], Thomas Shire[4]

1) Research Associate, Institute of Industrial Science, The University of Tokyo, 4-6-1 Komaba, Meguro-ku, Tokyo 153-8505, Japan. Email: otsubo@iis.u-tokyo.ac.jp (Corresponding Author)
2) Professor, Institute of Industrial Science, The University of Tokyo, 4-6-1 Komaba, Meguro-ku, Tokyo 153-8505, Japan. Email: kuwano@iis.u-tokyo.ac.jp
3) Professor, Department of Civil and Environmental Engineering, Imperial College London, Skempton Building, South Kensington Campus, Exhibition Road, London SW7 AQ1 2AZ, UK. Email: cath.osullivan@imperial.ac.uk
4) Lecturer, James Watt School of Engineering, University of Glasgow, Rankine Building, Glasgow G12 8QQ, UK. Email: thomas.shire@glasgow.ac.uk

Keywords: shear wave velocity; stiffness; frequency; discrete element method; gap-graded.

Word count (excluding Abstract and Reference list): 7248

Number of figures: 15

Number of tables: 4

Abstract

The behaviour of gap-graded granular materials, i.e. mixtures of coarse and cohesionless finer grains having a measurable difference in particle size, does not always confirm to established frameworks of sand behaviour. Prior research has revealed that the role of the finer particles on the stress-strain response, liquefaction resistance, and internal stability of non-cohesive gap-graded soils is significant and complex, and highly dependent on both the volumetric proportion of finer particles in the material and the coarse-particle to finer-particle size ratio. Quantifying the participation of the finer particles on the stress transmission and overall behaviour is central to understanding the behaviour of these materials. However, no experimental technique that can directly quantify the contribution of finer particles to the overall behaviour has hitherto been proposed. This paper explores to what extent the participation of finer particles can be assessed using laboratory geophysics, recognizing that granular materials act as a filter to remove the high frequency components of applied seismic / sound waves. Discrete element method simulations are performed to understand the link between particle-scale stress transmission and the overall response observed during shear wave propagation. When the proportion of finer particles is increased systematically both the shear wave velocity (V_S) and low-pass frequency (f_{lp}) increase sharply once a significant amount of the applied stress is transferred via the finer particles. This trend is also observed in equivalent laboratory experiments. Consequently, the f_{lp}–V_S relationship can provide useful insights to assess whether the finer particles contribute to stress transmission and hence the mechanical behaviour of the gap-graded materials.

List of symbols and notation

b	measure of the portion of the finer particles that contribute to the active intergrain contacts as proposed by Thevanayagam et al. (2002)
C_N	number contacts per particle (particle coordination number)
$\overline{C_N}$	mean coordination number
$\overline{C_N^{mech}}$	mean mechanical coordination number
$\overline{C_{N,c}^{cc,mech}}$	mean mechanical coordination number considering the number of coarse-coarse contacts that involve active coarse particles
$\overline{C_{N,c}^{cf,mech}}$	mean mechanical coordination number considering the number of coarse-finer particle contacts that involve active coarse particles
$\overline{C_{N,f}^{cf,mech}}$	mean mechanical coordination number considering the number of coarse-finer particle contacts that involve active finer particles
$\overline{C_{N,f}^{ff,mech}}$	mean mechanical coordination number considering the number of finer-finer particle contacts that involve active finer particles
D	particle diameter for coarse particles
D_{50}	median coarse particle diameter
D_{10}	10% of coarse particle diameters are smaller than D_{10}
d	particle diameter for finer particles
d_{50}	median finer particle diameter
e	global void ratio
e^{mech}	mechanical void ratio considering only active particles in the solid faction
e_g	intergranular void ratio
e^*	equivalent granular void ratio
e_{max}	maximum void ratio
e_{min}	minimum void ratio
F_C	fines content: total volume of finer particles/total volume of all particles
F_{thre}	threshold fines content
f_{lp}	low-pass frequency
f_{in}	nominal frequency of inserted signal
G_0	small-strain shear modulus
GN	narrowly gap-graded material
GW	widely gap-graded material
L	sample length
m	empirical constant in expression for e^* proposed by Thevanayagam et al. (2002)
N_p	number of particles
N_p^{mech}	number of active particles, i.e. particles with at least 2 contacts
$N_{p,c}^{mech}$	number of active coarse particles, i.e. coarse particles with at least 2 contacts
$N_{p,f}^{mech}$	number of active finer particles, i.e. finer particles with at least 2 contacts

N_C	number of contacts
N_c^{mech}	number of contacts considering only active particles
$N_{c,cc}^{mech}$	number of coarse-coarse contacts considering only active particles
$N_{c,cf}^{mech}$	number of coarse-finer particle contacts considering only active particles
$N_{c,ff}^{mech}$	number of finer-finer particle contacts considering only active particles
p'	isotropic stress level
R_d	size ratio, D_{50}/d_{50}
T_{travel}	time delay between inserted and received shear wave responses
V_S	shear wave velocity
V	total volume of particles
V_f	total volume of finer particles
V^k	volume of particle k
W	sample width
$\bar{\sigma}_{ff}^k$	mean stresses in particle k arising from finer-finer particle contacts acting on particle k
$\bar{\sigma}^k$	mean stresses in particle k arising from all contacts acting on particle k
μ_{prep}	inter-particle friction during sample preparation
μ_{wave}	inter-particle friction during wave propagation

Introduction

Cohesionless gap-graded materials are mixtures of coarse and cohesionless (non-plastic) finer grains having a gap or measurable difference between their sizes. It is generally accepted that the finer grains may exist in the void space between the coarse grains and not be involved in load transmission or the mechanical response of the material. Key factors governing the role of the finer particles on the mechanical response of gap-graded materials include the ratio of the median particle diameter of the coarse particles (D) to that of the finer particles (d), i.e. $R_d=D_{50}/d_{50}$, the volumetric fines content (F_C= total volume of finer particles/total volume of all particles) and the packing density (Shire et al., 2016). In the absence of plasticity or interparticle cohesion, it is appropriate to consider R_d rather than the absolute size of the finer particles. Many authors have discussed the concept of a threshold F_C value (F_{thre}) that distinguishes a material whose behaviour is determined by the coarse grains from a material whose behaviour is determined by the finer grains (Zuo and Baudet, 2015). The sensitivity of the mechanical response to F_C has been investigated in a number of prior studies (e.g. Lade and Yamamuro, 1997; Thevanayagam, 1998; Salgado et al., 2000; Rahman et al., 2008; Carraro et al., 2009) where an intergranular void ratio (e_g) that treats the volume of finer particles as part of the void space was considered for lower F_C values in place of global void ratio (e) as defined by Mitchell (1976):

$$e_g = \frac{e + F_C}{1 - F_C} \tag{1}$$

Thevanayagam et al. (2002) proposed an equivalent granular void ratio (e^*) which includes a parameter b (from 0 to 1) that quantifies the "portion of the fine grains that contribute to the active intergrain contacts":

$$e^* = \frac{e + (1-b)F_C}{1 - (1-b)F_C} \quad for\ F_C \leq F_{thre} \tag{2a}$$

$$e^* = \frac{e}{F_C + \frac{1 - F_C}{R_d^m}} \quad for\ F_C > F_{thre} \tag{2b}$$

where $0<m<1$; m is a constant that depends on grain characteristics and fine grain packing. Eq. 2a is applicable to a "fines in sand" case with $F_C \leq F_{thre}$, whereas Eq. 2b is used for the case of "sand in fines" with $F_C > F_{thre}$. Ni et al. (2004) and Rahman et al. (2008) proposed a semi-empirical equation to calculate b as a function of D_{10}/d_{50},

F_C and $F_{thre,}$ the threshold fines content. If all the finer particles are nonactive, b=0; Eq. 2a reduces to Eq. 1.

Gap-graded soils are susceptible to internal erosion by suffusion (e.g. Skempton and Brogan, 1994; Ke and Takahashi, 2014; Sato and Kuwano, 2015). Building on experimental work considering internal erosion by Skempton and Brogan (1994), Shire et al. (2014) investigated the role of the finer particles in stress transmission using the discrete element method (DEM) and found that, for the range of R_d values they considered, the finer particles just fill the voids between the coarse particles at a F_C value between 24% and 29%, with the exact F_{thre} depending on the sample packing density. Irrespective of the packing density, the finer particles separate the coarse particles so that they transfer significant stress at F_C values exceeding 35%. Similar transitional responses were also reported by Gong and Liu (2017) who also used DEM to analyse the packing characteristics of 2D circular and 3D spherical particles. An effective experimental technique to assess the contribution of the finer particles to overall stress transmission and hence the mechanical behaviour of the gap-graded soil has yet to be established.

The small-strain shear modulus of soil (G_0) is a key parameter to predict ground deformation, and it is often estimated using dynamic wave measurements (Atkinson, 2000; Clayton, 2011). Yang and Liu (2016) experimentally assessed the influence of F_C on the shear (S-) wave velocity (V_S) of gap-graded soils using bender elements and resonant column tests. Using binary mixtures of Toyoura sand and crushed silica fines (R_d=4) they found that V_S, and thus G_0, decreases as F_C increases up to F_C=30%. Choo and Burns (2015) conducted bender element tests using mixtures of Ottawa sand and finer grains with R_d=1.4, 3.6, 6.4 and 72 with a wide range of F_C values. Choo and Burns (2015) reported that increasing F_C reduces V_S and that a greater reduction in V_S is observed for larger R_d values. They reported a good correlation between V_S and e_g (Eq. 1) for F_C<F_{thre}. Goudarzy et al. (2016) found a good correlation between e^* and G_0 for mixtures of large and small spherical glass beads (R_d=10) at F_C≤50%. They observed that G_0 decreases as F_C increases for F_C≤30%, which was confirmed using DEM simulations by Gong et al. (2019). Goudarzy et al. (2016) also reported that G_0 increases at 40%≤F_C≤50%, showing what can be termed a transitional response over these F_C values. A similar transitional behaviour was observed by Otsubo et al. (2019) who tested loosely packed gap-graded glass bead

samples using both dynamic laboratory tests (using shear plates) and DEM simulations.

Granular materials act as a filter to remove the high frequency content of applied seismic/stress/sound waves. The maximum transmitted frequency, i.e. the low-pass frequency (f_{lp}), depends on the particle size, void ratio, and the confining stress (Santamarina et al., 2001; Mouraille and Luding, 2008; Otsubo et al., 2017a; Dutta et al., 2019). No prior study has examined the phenomenon of frequency filtering and f_{lp} in the case of gap-graded materials.

This contribution explores the role of non-cohesive finer particles on shear wave propagation in gap-graded materials using DEM simulations supplemented by experimental data. The F_C and e parameters are varied systematically to quantify both the state of packing and the mechanical response to applied stress waves considering two values of R_d parameters (Table 1). Referring to Tables 2 and 3, relatively large numbers of particles were considered (up to 2.3 million) to enable a representative element volume to be attained over a wide range of F_C values, while also ensuring that the sample size was large relative to the wavelength of the propagating wave. The ratio of sample length to median particle size ranges from approximately 85 to 750 in the longitudinal direction. Four states of packing in gap-graded soils are considered in this study referring to Thevanayagam et al. (2002):

- Case i: finer particles do not fill the voids between coarse particles and transfer negligible stress (Fig. 1a);
- Case ii: finer particles partially separate coarse particles at interparticle contacts creating a metastable structure, but do not fill the voids between coarse particles (Fig. 1b);
- Case iii: finer particles do not fill the voids between coarse particles but partially support the coarse matrix and transfer some stress (Fig. 1c);
- Case iv: finer particles fill the voids and separate coarse particles from one another (Fig. 1d).

Note that Case ii and Case iii in this study correspond to Case iii and Case ii, respectively, in Thevanayagam et al. (2002). Following Shire et al. (2014) Case i can be classified as underfilled fabric, Case iv is an overfilled

fabric and Cases ii and iii correspond to a density-dependent (transitional) fabric.

The following questions are considered in this contribution:

1) Does the proportion of finer particles and the proportion of stress transmitted by the finer particles affect the V_S, and thus the G_0, of gap-graded materials?
2) Can the participation of finer particles in the main fabric of gap-graded granular materials be assessed using laboratory geophysics testing?

These questions will be considered using data obtained from DEM simulations along with complementary experimental data.

DEM simulation approach

Materials and sample preparation

A modified version of the open-source DEM code granular LAMMPS (Plimpton, 1995) was used, simulations were run on the Oakforest-PACS high performance computing system operated by JCAHPC and software verification is documented in Otsubo (2016). Spherical particles were considered in the simulations to isolate the effects of F_C, R_d and e from the more complex correlations that might be induced by also considering particle shape effects. Shire et al. (2016) noted that the largest sphere which can fit within the void body of the densest face-centered cubic packing of uniform spheres (e=0.351) occurs at R_d≈4.45, but that a clear indication of bi-modal behaviour only occurs for $R_d \geq 6$. Thevanayagam et al. (2002) noted that Case i (Fig. 1a) is unlikely to occur when $R_d \leqq 6.5$ for mono-size coarse and finer particles. Therefore, two distinct values of R_d were considered in this study (Table 1):

a) Mixtures with finer particle diameters d= 0.4–0.65 mm and coarse particle diameters D= 1.2–2.2 mm (referred to here as narrowly gap-graded, GN) where R_d= 3.4, i.e. $R_d \leqq 6.5$
b) Mixtures of d= 0.15–0.25 mm and D= 1.2–2.2 mm (referred to here as widely gap-graded, GW) where R_d= 8.8, i.e. R_d>6.5

For each R_d value, target F_C values of 0%, 10%, 20%, 25%, 30%, 35%, 40%, 60%, 80% and 100% were

considered (Fig. 2a). Referring to Tables 2 and 3 the actual F_C values differ slightly from the nominal values; the data presented in the figures use the actual F_C values.

Typical material properties for alkaline glass beads were used in the simulations, so that the particle Young's modulus was 71.6 GPa, the Poisson's ratio was 0.23 and the specific gravity was 2.5. A simplified Hertz-Mindlin contact model with a Coulomb friction limit was used (Itasca, 2007). Similar to the approach adopted by Shire et al. (2014), the interparticle friction coefficients during isotropic compression (μ_{prep}) were set to be 0.01, 0.1, 0.25 for each sample type to vary the initial density, and the three resulting density levels are referred to here as dense, medium and loose, respectively. For the GN samples at an isotropic stress (p') of 50 kPa, an additional μ_{prep} value of 0.4 was used (very loose case) to enable comparison with the experimental data as will be discussed below. In total, 97 samples were simulated in this study. The number of particles in each sample depended on the sample type (either GN or GW), F_C and density. The maximum number of particles was about 2.3 million for the GW samples.

Samples were bounded by rigid wall boundaries in the longitudinal (Z-) direction and periodic boundaries in the horizontal (X- and Y-) directions (Fig. 2b). To create each sample a cloud of non-contacting particles was first generated, and a servo-control was applied to the boundaries to compress the sample to either p'=50 kPa or 100 kPa. A small amount of viscous damping was applied after the target stress level was achieved to remove particle kinetic energy. The length (L) of the samples ranged from 128 mm to 159 mm, and the lateral width (W) ranged from 3.6 mm to 22.0 mm (Tables 2 and 3). In all cases at least 10 particles were placed orthogonal to the directions of the periodic boundaries, and the longitudinal length was selected to be similar to the physical samples considered in the complementary experiments discussed below. Examples of medium dense packings of a middle core (10×10×10 mm) for the GN and GW samples with F_C=10%, 20% and 30% are illustrated in Fig. 3 where C_N stands for the number of contacts per particle. No gravitational force was applied in the simulations to prevent segregation of the coarse and finer particles.

Shear wave propagation approach

The planar *S*-wave propagation simulation procedure broadly followed that documented in Otsubo et al. (2017b) and Otsubo and O'Sullivan (2018), where simulations of laboratory dynamic tests using planar piezoceramic transducers were considered (Brignoli et al., 1996; Suwal and Kuwano, 2013; Ismail and Rammah, 2005; Otsubo and O'Sullivan, 2018; Dutta et al. 2019). In contrast to conventional bender element tests (Shirley and Hampton, 1978) this approach can generate planar *S*-waves. The viscous damping used during the isotropic compression was turned off during wave propagation. The μ_{prep} values were increased to μ_{wave}=0.5 prior to the stress wave propagation to prevent particle sliding at contacts during the wave propagation following Magnanimo et al. (2008). A check was made to confirm that further increases in μ_{wave} did not influence the dynamic wave signals. The bottom "transmitter" wall was translated horizontally in the X-direction, and *S*-waves propagated vertically to the top "receiver" wall. The translational displacement of the transmitter wall was controlled to be a single period sinusoidal pulse with a double amplitude of 5 nm. The resultant changes in shear stress on both the transmitter and receiver walls were recorded to determine both V_S and f_{lp}. To determine the optimal nominal input wave frequency f_{in}, an experimental parametric study was carried out in which f_{in} was systematically varied. The frequency that produced the greatest maximum amplitude in the frequency domain response of the received signal was found to be about 7 kHz. Maximizing the signal-to-noise ratio in this way improves signal quality and the reliability of the resulting V_S data (Dutta et al., 2019). This approach is often used to minimize the discrepancy between the start-to-start method and the peak-to-peak method in experimental research, e.g. Yamashita et al. (2009). However to determine the f_{lp} a broader range of nominal input signal frequencies including higher frequency wave components was required and so in these cases f_{in}=50 kHz or 100 kHz.

Complementary laboratory experiments

Sample preparation

To verify the physical relevance of the DEM simulation results, a series of complementary laboratory

experiments were completed using glass ballotini having particle sizes and material properties equivalent to the DEM-GN samples. The shape of the glass ballotini was close to, but not exactly spherical; measurements using a QICPIC apparatus gave a sphericity (S) of 0.943, aspect ratio (AR) of 0.962, and (C) convexity of 0.988 for the coarse particles, and S=0.940, AR=0.975 and C=0.974 for the finer particles using the shape measures explained in Altuhafi et al. (2013). The surface of particles was nominally smooth having a root mean square of surface roughness of 45 nm for the coarse particles. In the experiments, five F_C values were considered, i.e. F_C=0%, 20%, 40%, 60% and 100%. A customized method of sample preparation was adopted to reduce segregation of coarse and finer particles while enabling a study of the effect of packing density on the sample responses. The mixtures of coarse and finer particles were poured carefully under dry conditions into a metal mould using a funnel. The funnel was slowly lifted during the pouring process so that the elevation of the tip of the funnel was always kept just above the sample surface. These loosely prepared samples were compressed to p'=50 kPa by applying a vacuum confinement. After measuring the dimensions of the sample (almost 75 mm in diameter, 156 mm in height), dynamic wave propagation experiments were performed as detailed below. Upon completion of the wave propagation test, the tested sample was again enclosed within the metal mould, the vacuum confinement was gradually reduced and once the effective stress reduced to zero the topcap was carefully removed. The sample density was then increased by repeatedly hitting the side of the metal mould. After a selected mass was added to the top of the sample, the afore-mentioned process was repeated up to four times; varying the magnitude of this mass and number of side blows enabled a range of densities to be considered. The experiments were terminated when further vibration cannot densify the sample effectively. In total four or five densities were prepared for each fines content, and the loosest and densest samples are referred to here as *dense and loose* samples, whereas the other samples are referred to here as *intermediate* samples. These void ratio values do not directly relate the void ratio values of the DEM samples; the dense samples tested in the laboratory were looser than the dense samples in DEM simulations. The ranges of e values tested in the laboratory were 0.597–0.662 for F_C=0%, 0.434–0.511 for F_C=20%, 0.414–0.507 for F_C=40%, 0.459–0.523 for F_C=60%, and 0.594–0.670 for F_C=100%. Referring to Cho et al. (2006), the range of attainable void ratios is narrow for particles that are spherical or close to spherical. During the sample preparation process, segregation

of coarse and finer particles was not obvious for the GN mixtures with R_d=3.4.

Shear wave measurements

The dynamic wave testing procedure adopted in the experiments followed Dutta et al. (2019). Disk-shaped *S*-type planar piezoceramic transducers (20 mm in diameter and 2 mm in thickness) were installed inside the base pedestal and topcap. These transformers have a polarization in the horizonal direction normal to the direction of wave propagation and they directly contacted the top and bottom of the sample to insert or receive *S*-waves. The *S*-waves were generated using a digital function generator wih a bipolar amplifier. A single period sinusoidal pulse waveform with a double amplitude of 70 V was inserted at the topcap, and the received signals at the base pedestal were recorded using an oscilloscope. As in the DEM simulations, two f_{in} values were used: f_{in}=7 kHz for the tests to determine V_S, and f_{in}≈50 kHz for the tests to determine f_{lp}. The maximum translational displacements measured in air were approximately 50 nm for f_{in}=7 kHz, and 10 nm for f_{in}=50 kHz, as detailed in Dutta (2019).

Analyses of packing characteristics

Void ratio and mean coordination number

The variations in global void ratio (e) with F_C for all the packing densities considered are illustrated in Fig. 4. Referring to Fig. 4a for each sample with a mixture of particle sizes at p'=100 kPa, the GW samples give lower e values when compared to the GN samples for a given F_C in line with Shire et al. (2016). The minimum e is observed at F_C=25% for the dense and medium cases, and F_C=30% for the loose case for both the GW and GN samples. These minimum points are sometimes used to determine the threshold fines content as summarised in Zuo and Baudet (2015). The influence of stress level on e was insignificant as confirmed by comparing data for the GN samples for simulations using 100 kPa and 50 kPa (Figs. 4a and 4b). For the laboratory samples, the range of e values tested were larger than that for the DEM equivalents (Fig. 4c). This difference in void ratio is explained partially by the difference in the sample preparation where the laboratory samples were prepared loosely using air-pluviation followed by side tapping, causing a slight difference in packing

geometry. Furthermore, the shape of glass beads is not perfectly spherical, in contrast to the DEM equivalents. The minimum and maximum void ratios (e_{min} and e_{max}) for F_C=0%, 20%, 30%, 40%, 60% and 100% were measured following the JGS standard (JGS 0161, 2009), where a slightly larger container (60 mm high and 80 mm in diameter) was used to test particle sizes larger than 2 mm. The variations of e_{min} and e_{max} with F_C are illustrated in Fig. 4c where the laboratory dense samples almost correspond to e_{min} for each F_C value.

Using the DEM simulation data, the influence of F_C on the mean coordination number ($\overline{C_N}$) (mean number of contacts per particle) for the GN and GW samples at p'=100 kPa is summarised in Fig 5a. As the properties of the coarse and finer grains (other than particle size) are the same, the e and $\overline{C_N}$ values are similar at F_C=0% and 100% for each density considered. For each material, a denser sample gives a higher $\overline{C_N}$ at a given F_C; however, the variation of $\overline{C_N}$ with F_C is complex. In all cases $\overline{C_N}$ drops sharply as the F_C increases from 0% to 10%. For the GN samples, $\overline{C_N}$ increases gradually once F_C>10%. The GN samples at p'=50 kPa give $\overline{C_N}$ values that were only slightly lower than those for the GN samples at p'=100 kPa and the overall trend was the same. For the GW samples, $\overline{C_N}$ rises sharply at F_C=25%, 30% and 35% for the dense, medium and loose cases, respectively. These sudden changes occur as finer particles having 0 or 1 contact points (referred to here as non-active particles) exist when the fabric is underfilled at F_C<25% (Fig. 1a) but as F_C increases and the fabric transitions to be overfilled the proportion of non-active finer particles greatly reduces.

Following Thornton (2000), the mean mechanical coordination number ($\overline{C_N^{mech}}$) was calculated by excluding the number of contacts involving the non-active particles as below:

$$\overline{C_N^{mech}} = \frac{2\left(N_c - N_c^{C_N<2}\right)}{N_p - N_p^{C_N<2}} \tag{3}$$

where N_c and N_p are the total number of contacts and particles, respectively, $N_p^{C_N<2}$ stands for the number of non-active particles that have C_N values of 0 or 1 and $N_c^{C_N<2}$ is the number of contacts involving non-active particles.

Referring to Fig. 5b, the $\overline{C_N^{mech}}$ values are not sensitive to F_C for the GN samples, implying a unique relationship between μ_{prep} and $\overline{C_N^{mech}}$. A drop in $\overline{C_N^{mech}}$ is observed for the GW samples with around

F_C=25%. The drop was observed because a considerable number of finer particles having only two contacts with coarse particles exist, indicating a metastable packing linking to Case ii (Fig. 1b) as discussed below. The mechanical void ratio (e^{mech}) was determined by considering the volume of non-active particles to contribute to the void volume (Fig. 5c). For the GN samples, e^{mech} reduces gradually with increasing F_C for F_C>10% until F_C≈50% at which point e^{mech} starts to gradually increase with increasing F_C. In contrast, for the GW samples, e^{mech} drops sharply at F_C=25%, 30% and 35% for the dense, medium and loose cases, respectively, followed by a gradual increase in e^{mech} with subsequent increases in F_C. A summary of the F_{thre} values determined using the minimum values of each measure of packing status is provided in Table 4.

Variation in contact types

The $\overline{C_N^{mech}}$ value can be decomposed into four contact types (Fig. 6): (a) the average number of coarse-coarse contacts per coarse particle ($\overline{C_{N,c}^{cc,mech}} = 2N_{c,cc}^{mech}/N_{p,c}^{mech}$), (b) the average number of coarse-finer particle contacts per coarse particle ($\overline{C_{N,c}^{cf,mech}} = N_{c,cf}^{mech}/N_{p,c}^{mech}$), (c) the average number of coarse-finer particle contacts per finer particle ($\overline{C_{N,f}^{cf,mech}} = N_{c,cf}^{mech}/N_{p,f}^{mech}$), (d) the average number of finer-finer particle contacts per finer particle ($\overline{C_{N,f}^{ff,mech}} = 2N_{c,ff}^{mech}/N_{p,f}^{mech}$). N_c^{mech} stands for the total number of force-transmitting (i.e. active) contacts involving active particles for the contact type indicated, N_p^{mech} stands for the number of active particles and the subscripts/superscripts of *c* and *f* stand for coarse and finer, respectively. The $\overline{C_{N,c}^{cc,mech}}$ value decreases as F_C increases (Fig. 6a) as the finer particles push the coarse particles apart. This reduction is monotonic for the GN samples for F_C>0%, however in the GW samples $\overline{C_{N,c}^{cc,mech}}$ is insensitive to F_C for low F_C values and only starts to decrease at 20%<F_C<30%. The variation in $\overline{C_{N,f}^{ff,mech}}$ with F_C is almost a mirror image of the $\overline{C_{N,c}^{cc,mech}}$ data but the change in $\overline{C_{N,f}^{ff,mech}}$ is particularly sharp in the GW samples (Fig. 6d). Referring to Fig. 6b, the maximum value of $\overline{C_{N,c}^{cf,mech}}$ depends on R_d; $\overline{C_{N,c}^{cf,mech}}$ exceeds 200 for the dense GW sample with F_C=80%, while the maximum $\overline{C_{N,c}^{cf,mech}}$ was 35 for the dense GN samples. The $\overline{C_{N,f}^{cf,mech}}$

value quantifies the number of coarse-finer particle contacts relative to $N_{p,f}^{mech}$ is also determined by R_d (Fig. 6c). The maximum $\overline{C_{N,f}^{cf,mech}}$ value is approximately 3.5 for the GN samples (R_d=3.4), and 2 for the GW samples (R_d=8.8) where geometric considerations mean that a finer particle cannot contact three or more coarse particles simultaneously. The clear maximum $\overline{C_{N,f}^{cf,mech}}$=2 for the GW sample with F_C=20% indicates that the finer particles are just starting to separate the coarser grains as there are many finer particles acting alone to separate two coarse particles; this would correspond to Case ii (Fig. 1b).

Stress transmission through finer particles

To assess the participation of the finer particles in the mechanical behaviour, two indices were considered (i) α^{ff} which quantifies the proportion of stress transmitted by the finer-finer particle contacts only and (ii) α (as defined by Shire et al. (2014)) which considers the proportion of stress transmitted by the finer particles (i.e. considering both coarse-finer particle and finer-finer particle contacts) as follows:

$$\alpha^{ff} = \frac{V}{V_f}\frac{\sum_{k=1}^{N_{p,f}}(\bar{\sigma}_{ff}^{k}\,V^k)}{\sum_{k=1}^{N_p}(\bar{\sigma}^k\,V^k)} \tag{4a}$$

$$\alpha = \frac{V}{V_f}\frac{\sum_{k=1}^{N_{p,f}}(\bar{\sigma}^k\,V^k)}{\sum_{k=1}^{N_p}(\bar{\sigma}^k\,V^k)} \tag{4b}$$

where V^k is the volume of particle k, and V_f and V are the total volume of finer particles and the total volume of all particles respectively, $N_{p,f}$ and N_p are the total number of finer particles and the total number of all particles respectively, and $\bar{\sigma}_{ff}^{k}$ and $\bar{\sigma}^k$ are the mean stresses in particle k arising from finer-finer particle contacts and from all contacts acting on particle k respectively.

Figure 7 shows the variations in both α^{ff} and α with F_C; the values differ as α includes the contribution from coarse-finer particle contacts. Comparing Figs. 7a and 6d for the GN samples, α^{ff} increases gradually as F_C increases, just as $\overline{C_{N,f}^{ff,mech}}$ varies with F_C. For the GW samples, α^{ff} remains almost zero until a sharp rise

takes place at F_C=25%, 30% and 35% for dense, medium and loose cases, respectively. These data support the finding of Shire et al. (2014) that the specific point at which the finer particles make a measurable contribution to mechanical behaviour depends on density as well as on F_C and R_d. For the GN samples (R_d=3.4), Case i (Fig. 1a) is unlikely to occur, consequently the finer particles of the GN samples are expected to carry some stress even at small F_C values (Case iii, Fig. 1c). For F_C>40%, the α^{ff} values for the GW samples exceed those for the GN samples and decrease monotonically. The GW samples having a larger R_d give a more distinct transition to a fine-dominated response, which agrees in general with the experimental observations for sands synthesized by Zuo and Baudet (2015). The finer particles in the GN samples are too large to fit into a void constructed by four close-packed coarse particles and so the transition is rather smooth because even a small proportion of finer particles will restrict contact formation between coarse particles. In contrast, the finer particles in the GW samples are sufficiently small to fit into a void constructed by closely packed coarse particles so that at low F_C values the finer particles do not disturb coarse particle fabric; however contacts between coarse particles will no longer occur once the void is completely filled by finer particles. Therefore, the increase in α is closely linked to the reduction in $\overline{C_{N,c}^{cc,mech}}$ (Fig. 6a) at lower F_C values in line with observations in Shire et al. (2016). Table 4 summarises the F_{thre} values at which a sharp increase/decrease in characteristics of each packing or mechanical response occurs, departing from being underfilled towards overfilled.

The measures α^{ff} and α consider the finer particles only, a more comprehensive appreciation can be gained by decomposing the macroscale stress tensor into three partitions that depend on the contact type: (a) coarse-coarse, (b) coarse-finer and (c) finer-finer particle contacts as illustrated in Fig. 8 for the dense GW and GN samples for each F_C value considered. The proportion of stress transmitted by the coarse-coarse particle contacts reduces as the finer particles become more engaged in stress transmission. The reduction in the proportion of stress transmitted by the coarse-coarse particle contacts correlates clearly with the increase in the α values illustrated in Fig. 7b.

Sample responses to shear wave propagation

Shear wave velocity

As outlined above, f_{in}=7 kHz was used to determine V_S. The time-domain shear stress responses at the transmitter and receiver (where time values normalised by the travel distance, L) are illustrated in Fig. 9. Considering the densest cases for each test series, the variations in the sample responses with F_C are similar for F_C=0%, 20% and 100% irrespective of the considerable differences in e, while an earlier arrival of S-waves is evident for F_C=40%. Referring to Fig. 9d for the experimental data, the order of wave arrival agrees with the DEM equivalents at p'=50 kPa (Fig. 9c), the slightly lower wave velocities are explained by the lower sample densities when compared with the DEM simulations.

The peak-to-peak method (Yamashita et al., 2009; Dutta et al., 2019) was adopted to determine the wave travel time (T_{travel}) where the time delay between the first peaks of the transmitter and receiver responses gives T_{travel} and $V_S=L/T_{travel}$; this approach gives a close match with V_S data based on particle-scale displacement values as reported in Otsubo et al. (2017b). The influence of F_C on V_S is considered in Fig. 10 where the V_S values increase with density at each F_C values for both the GN and GW samples. When samples with F_C=0% and 100% are compared, equivalent values of V_S are seen for both the GN and GW samples in the DEM simulations. For the DEM data the dense and medium GN samples experience an increase in V_S between F_C=20% and 40%, while the loose samples exhibit an initial reduction in V_S at F_C=20% and 25%, followed by an increase in V_S up to F_C=60%. Similar but more marked variations can be seen for the GW samples; the V_S values for the dense and medium samples increase at F_C=30%, while the loose sample shows a measurable reduction in V_S at F_C=30%, followed by a sharp increase at F_C=35%. The variations in V_S with F_C seem to have an opposite trend when compared to the variations in e^{mech} with F_C as shown in Fig. 5c. Figs. 10b and 10c compare DEM and experimental data where the V_S data points for experimental results are bounded between very loose and medium dense of DEM equivalents. Note that for a given e value, the laboratory data for V_S tend to appear lower than the DEM equivalents as imperfections in the glass beads and the finite roughness of their surfaces result in a lower effective contact stiffness (Cavarretta et al., 2012; Otsubo and O'Sullivan, 2018). In the DEM

– experimental studies documented in O'Donovan et al. (2016) and Otsubo and O'Sullivan (2018), a reduced Young's modulus, E, was used. However it is difficult to accurately decide by how much to reduce E and so the current DEM study used the material properties provided by the manufacturer.

To explore the link between V_S and packing density, V_S is plotted against e for the DEM simulations with p'=100 kPa in Fig. 11. V_S varies with both F_C and e, and the variation is more significant for the GW samples (Fig. 11b). The monodisperse materials (F_C=0% and 100%) exhibit the same relationship between V_S and e. The V_S–e relationship shifts leftward as F_C increases for 0%<F_C≤30%. This trend agrees with experimental findings using gap-graded soils with R_d=4 (Yang and Liu, 2016). However, further increases in F_C shift the V_S–e relationship to the right and back to the original (monodisperse) relationship between V_S and e. This non-trivial behaviour has been also reported in the laboratory experiments using mixtures of glass beads with R_d=10 by Goudarzy et al. (2016) and mixtures of natural sands with R_d= 3.6, 6.4 and 72 (Choo and Burns, 2015). Fig. 11 indicates that V_S is not a function of e alone when gap-graded mixtures are considered. Hardin and Richart (1963) established a fundamental framework for the V_S–e relationship informed by experimental data; a review of those data indicates that the gap-graded Ottawa sand mixture they considered does not completely confirm with the trends they observed for monodisperse materials.

There is a more coherent relationship between V_S and e^{mech} as illustrated in Fig. 12a. Previous research has demonstrated that there is a close relationship between the small-strain shear modulus and $\overline{C_N^{mech}}$ for a given void ratio (Makse et al., 1999; Magnanimo et al., 2008). The data points located below the best-fit relationship in Fig. 12a, particularly for the GW loose cases, can be related to the low connectivity (Fig. 5b), and the metastable Case ii fabric when finer particles just separate coarse particles. Effective medium theory indicates V_S should correlate with a function of $\overline{C_N^{mech}}/(1+e^{mech})$ (Yimsiri and Soga, 2000), and this indeed gives very strong correlation with V_S (Fig. 12b). However, these variables cannot be measured in the laboratory, limiting the practical value of this observation in interpreting experimental data. Although e^* in Eq. 2 does not directly correspond to the e^{mech} parameter in the present analyses, the concept of using an effective void ratio as proposed by Thevanayagam et al. (2002) and Rahman et al. (2008) to V_S seems to be appropriate when gap-graded

materials are discussed.

Low-pass frequency

Granular materials act as a filter to sound or stress waves (Santamarina et al., 2001; Mouraille, 2009; Lawney and Luding, 2014) so that frequencies higher than the low-pass frequency (f_{lp}) do not propagate through the material. f_{lp} is a material property that is influenced by packing density, effective stress and particle size (Otsubo et al., 2017a; Dutta et al., 2019). The frequency domain responses for the shear stresses recorded at the boundary walls for dense samples are compared in Fig. 13a for the DEM-GN samples and Fig. 13b for the DEM-GW samples at p'=100 kPa. At each frequency considered, the gain factor is defined as the amplitude of the fast Fourier transform (FFT) of the received signal / the amplitude of the FFT of the inserted signal. Generally, at low frequencies larger gain factor amplitudes with multiple local resonances are observed, while the amplitudes reduce with increasing frequency. The f_{lp} value was taken to be the frequency at which the amplitude of gain factor drops beneath a threshold gain factor value and where there is no additional larger amplitude gain factor at higher frequencies (Otsubo et al., 2017a; Dutta et al., 2019). The threshold gain factor value adopted here was of 2×10^{-6} for the experiments and 0.04 for the DEM simulations; the difference in the threshold values chosen is due to the more significant energy loss observed in experiments where electrical voltage is converted to force and vice versa, as discussed in Dutta et al. (2019). Comparing Figs. 13a and 13c for the GN samples, while the threshold, low-pass frequencies are larger for p'=100 kPa the overall variation of f_{lp} with F_C is similar. Referring to Fig. 13d, the experimental data inevitably contain some noises and multiple resonances due to the system stiffness, configuration of piezoceramics and boundary conditions, particularly at lower frequencies. However, a threshold or low-pass frequency can be identified in the experimental data and its variation with stress is comparable with the f_{lp} stress-dependency observed in the equivalent DEM simulations.

Using both experiments and DEM simulations, Dutta et al. (2019) found that assemblies comprising of smaller grains exhibit a greater f_{lp} value. The packing density also affects the f_{lp} value; Otsubo et al. (2017a) considered DEM analyses and reported an increase in f_{lp} with an increase in packing density for 3D monodisperse systems.

For the gap-graded mixtures considered in this study, Fig. 14 shows the relationship between f_{lp} and F_C. For both the GN and GW (DEM and laboratory) samples, at a given F_C, f_{lp} increases with packing density. For the GN samples, considering both the DEM and laboratory test data, f_{lp} increases with increasing F_C and a transition marked by a more rapid increase in f_{lp} is evident at $20\% \leq F_C \leq 40\%$. A denser packing leads to an earlier transition, i.e. at a lower F_C corresponding to a lower F_{thre}. The lower p' value of 50 kPa gives lower f_{lp} values; in agreement with the effect of f_{lp} observed in the DEM study by Otsubo et al. (2017a). On the other hand, for the GW samples, the medium and loose DEM samples show a measurable drop in f_{lp} up to F_C=25% and 30%, respectively (Fig. 14a), consistent with the trend observed in the variation in α^{ff} and V_S (Figs. 7a and 10a). The f_{lp} for dense, medium and loose cases increase sharply at F_C=25%, 30% and 35% respectively, corresponding to their F_{thre} values (Table 4). For F_C>30% the dense case exhibits a gradual decrease in f_{lp} with increases in F_C, probably due to an increase in e (Fig. 4a), followed by a sharp rise at F_C=100%.

Discussion

As discussed above, V_S, f_{lp}, e^{mech} and α^{ff} are all closely linked, and the correlations between V_S and e^{mech} and between f_{lp} and α^{ff} are particularly clear. However, e^{mech} and α^{ff} cannot be measured in laboratory tests. To use the DEM observations to inform the interpretation of laboratory test data, the f_{lp}–V_S relationship was investigated, and the following observations can be made.

GN samples with a low R_d value ($R_d \leqq 6.5$)

The f_{lp}–V_S relationship for both the GN and GW samples is presented in Fig. 15 where the colour of each data point of DEM simulations indicates the α^{ff} value for the relevant sample. Referring to Fig. 15a for the GN samples at p'=100 kPa, for each F_C considered the f_{lp}–V_S relationship is almost linear, with the data points for denser cases being located at the upper right side for each trend line. The slope of the linear f_{lp}–V_S relationship gradually increases as F_C increases, so that, for a given V_S, f_{lp} increases with F_C systematically. The α^{ff} value also increases systematically as F_C increases. For F_C=0% and 10% the GN samples give a similar f_{lp}–V_S relationship, indicating an underfilled (Case i, Fig. 1a) fabric with α^{ff}<0.1. The GN samples with

20%≤F_C≤25% give a transitional (Case iii, Fig. 1c) fabric, and start shifting to an overfilled (Case iv, Fig. 1d) fabric with α^{ff}>0.5 at F_C≥30% depending on the relative density. Fig. 15b compares the experimental data and DEM data at p'=50 kPa. These GN samples at p'=50 kPa give a similar variation to p'=100 kPa dataset. For a given F_C, the DEM simulations and the experimental data give a similar f_{lp}–V_S relationship, highlighting that the present DEM results capture the observations in the laboratory. Referring to Otsubo et al. (2017a) both V_S and f_{lp} are affected by void ratio, so that the f_{lp}–V_S relationship presented here can be mostly depends on α^{ff} which in turn depends on the combined effects of F_C and density.

GW samples with a large R_d value (R_d>6.5)

For the GW samples in Fig. 15c, the data points at F_C≤20% coincide with the trend for F_C=0%, marking a lower bound for the f_{lp}–V_S relationship, where the stress transmission via finer-finer particle contacts is negligible (α^{ff}≈0, Fig. 7a), i.e. referring to Fig. 1a there is an underfilled (Case i) fabric. A slight increase in F_C alters the fabric from underfilled to a Case ii transitional where finer particles start to separate the coarse particles (Fig. 1b) or a Case iii (Fig. 1c); the onset of this transition depends on the relative density of sample. The data points in the metastable Case ii zone correspond to points where $\overline{C_{N,f}^{cf,mech}}$=2 (Fig. 6c) and where both the V_S and f_{lp} values are lower than the cases for F_C=0%. The data points in Case iii corresponds to larger V_S and f_{lp} values. Further increases in F_C give a larger f_{lp} for a given V_S value, where finer particles start dominating the fabric, i.e. the fabric becomes overfilled (Case iv). The data points for F_C=100% deviate significantly from that for 30%≤F_C≤80%. As reported in Dutta et al. (2019), f_{lp} increases inversely with the D_{50} of monodisperse samples; the considerable increase in f_{lp} for F_C=100% can be explained due to the size ratio R_d=8.8.

Use of f_{lp}–V_S relationship to identify contribution of finer particles to stress transmission

Based on the data analysis above the following approach is proposed as means to assess whether or not finer particles are participating in the main, stress transmitting fabric in experimental studies:

1. Determine the f_{lp}–V_S relationship for samples composed of coarse particles only (F_C=0%). The resulting approximately linear trend observed gives a lower bound to the f_{lp}–V_S relationship.

2. Carry out laboratory element tests on the gap-graded materials of interest to determine both V_S and f_{lp} for these samples.
3. Gap-graded samples where the finer particles transmit less than 10% of the stress (i.e. with α^{ff}<0.1) will generate data points that are close to the f_{lp}–V_S relationship for F_C=0%. These samples are classified as having an underfilled fabric (Case i, Fig. 1) whose response will be determined by the characteristics of the coarse particles (i.e. F_C=0%).
4. The samples with 0.1≤α^{ff}<0.5 give an intermediate response so that the combined V_S and f_{lp} values lie along the trendline obtained for the α^{ff}<0.1 samples, but beyond the limits of those data points. If a data point has a combined V_S and f_{lp} that is below and to the left of the range for F_C=0%, referring to Fig. 1b the sample has a Case ii fabric, i.e. individual finer particles are just separating the coarse grains. If a data point lies to the above or right of the range for F_C=0%, the tested sample is transitional but stable (Case iii, Fig. 1c).
5. In the case of samples where the finer particles transmit more than 50% of the stress (i.e. α^{ff}≥0.5) and thus have an overfilled fabric (Case iv) the f_{lp} values at a given V_S lie measurably above the α^{ff}<0.1 data and the range of V_S values attained is significantly broader than those observed for F_C=0%.

The present study only considers gap ratios up to R_d=8.8. The contrast between coarse-dominated and fine-dominated behaviour becomes more marked as R_d increases, leading to an easier interpretation of the state of packing whether underfilled, transitional or overfilled. Further DEM studies with a larger R_d would require substantial computational effort. Referring to Table 4, the F_{thre} value is more obvious and consistent for the GW samples; 20%≤F_{thre}≤25% for the dense samples, 25%≤F_{thre}≤30% for the medium samples, 30%≤F_{thre}≤35% for the loose samples irrespective of types of physical or mechanical properties including e, e^{mech}, $\overline{C_N}$, α^{ff}, α, V_S and f_{lp}. However, for the GN samples F_{thre} depends on property being measured as shown in Table 4 and also noted by Zuo and Baudet (2015). This contribution has considered mixtures of cohesionless (non-plastic) spherical particles; the conclusions should not be extrapolated to mixtures containing cohesive (plastic) fines without appropriate experimental examination. If the coarse and finer particles have different elastic properties,

the f_{lp}–V_S relationships for F_C=0% and F_C=100% cases should be obtained firstly so that the f_{lp}–V_S relationship of their mixtures can be investigated in a relative manner.

Conclusions

This study has assessed the participation of non-cohesive finer particles in the main fabric of cohesionless gap-graded materials and considered the small-strain dynamic responses of these materials. The responses observed in DEM simulations using 97 samples with up to approximately 2.3 million particles were considered. The physical relevance of the observations was confirmed via complementary laboratory experiments. The following conclusions can be drawn from this contribution.

- The variation of V_S with F_C for gap-graded materials is complex and the nature of the variation depends on R_d. However the V_S values for all samples considered here have a clear correlation with e^{mech}; an even stronger correlation is observed between V_S and $\overline{C_N^{mech}}/(1+e^{mech})$ in line with prior studies of materials with monodisperse or continuous gradings. These data demonstrate the shortcomings of using e as a measure of state and highlight the need for experimental techniques to better understand the extent to which the finer particles participate in stress transmission.
- The low-pass frequency, $f_{lp,}$ increases sharply when finer particles start dominating the stress transmission; the point at which $f_{lp,}$ increases sharply coincides with the point at which the α^{ff} value, a measure of the stress in the finer particles, also increases sharply. A higher f_{lp} value indicates that the elastic waves are propagating via force chains comprising finer particles.
- For gap-graded mixtures plotting the f_{lp}–V_S relationship enables assessment of whether the finer particles contribute to the main fabric or not, without knowing the internal fabric parameters such as e^{mech} or α^{ff} provided that the f_{lp}–V_S relationship for samples of coarse particles alone (i.e. F_C=0%) with different packing densities is known.

Acknowledgements

This work was supported by the special fund of Institute of Industrial Science, The University of Tokyo, and by JSPS KAKENHI Grant Number 19K15084. The simulations presented in this contribution were performed using the Fujitsu PRIMERGY CX600M1/CX1640M1 (Oakforest-PACS) in the Information Technology Center, The University of Tokyo. Modifications to the LAMMPS molecular dynamics code by Dr. Kevin J. Hanley, The University of Edinburgh, enabled this research.

References

Altuhafi, F., O'Sullivan, C., Cavarretta, I., 2013. Analysis of an image-based method to quantify the size and shape of sand particles. Journal of Geotechnical and Geoenvironmental Engineering 139 (8), 1290–1307. https://doi.org/10.1061/(ASCE)GT.1943-5606.0000855

Atkinson, J.H., 2000. Non-linear soil stiffness in routine design. Géotechnique 50 (5), 487–508. https://doi.org/10.1680/geot.2000.50.5.487

Brignoli, E., Gotti, M., Stokoe, K., 1996. Measurement of shear waves in laboratory specimens by means of piezoelectric transducers. Geotechnical Testing Journal 19 (4), 384–397. https://doi.org/10.1520/GTJ10716J

Carraro, J.A.H., Prezzi, M., Salgado, R., 2009. Shear strength and stiffness of sands containing plastic or nonplastic fines. Journal of Geotechnical and Geoenvironmental Engineering 135 (9), 1167–1178. https://doi.org/10.1061/(ASCE)1090-0241(2009)135:9(1167)

Cavarretta, I., O'Sullivan, C., Ibraim, E., Lings, M., Hamlin, S., Muir Wood, D., 2012. Characterization of artificial spherical particles for DEM validation studies. Particuology, 10 (2), 209–220. https://doi.org/10.1016/j.partic.2011.10.007

Cho, G.C., Dodds, J., Santamarina, J.C., 2006. Particle shape effects on packing density, stiffness, and strength: natural and crushed sands. Journal of Geotechnical and Geoenvironmental Engineering 132 (5), 591 − 602. https://doi.org/10.1061/(ASCE)1090-0241(2006)132:5(591)

Choo, H., Burns, S.E., 2015. Shear wave velocity of granular mixtures of silica particles as a function of finer fraction, size ratios and void ratios. Granular Matter, 17, 567–578. https://doi.org/10.1007/s10035-015-0580-2

Clayton, C.R.I., 2011. Stiffness at small strain: research and practice. Géotechnique 61 (1), 5–37. https://doi.org/10.1680/geot.2011.61.1.5

Dutta, T.T., Otsubo, M., Kuwano, R., O'Sullivan, C., 2019. Stress wave velocity in soils: Apparent grain-size effect and optimum input frequencies. Géotechnique Letters 9 (4), 340–347. https://doi.org/10.1680/jgele.18.00219

Dutta, T.T., 2019. Effects of grain characteristics on anisotropic mechanical properties evaluated by elastic waves. The University of Tokyo, Tokyo, Japan, Ph.D. thesis.

Gong, J., Liu, J., 2017. Mechanical transitional behavior of binary mixtures via DEM: Effect of differences in contact-type friction coefficients, Computers and Geotechnics 85, 1–14. https://doi.org/10.1016/j.compgeo.2016.12.009

Gong, J., Wang, X., Li, L., Nie, Z., 2019. DEM study of the effect of fines content on the small-strain stiffness of gap-graded soils, Computers and Geotechnics 112, 35–40. https://doi.org/10.1016/j.compgeo.2019.04.008

Goudarzy, M., König, D., Schanz, T., 2016. Small strain stiffness of granular materials containing fines, Soils and

Foundations 56 (5), 756–764. https://doi.org/10.1016/j.sandf.2016.08.002

Hardin, B.O., Richart, Jr. F.E., 1963. Elastic wave velocities in granular soils. Journal of the Soil Mechanics and Foundations Division 89 (1), 33–65.

Ismail, M.A., Rammah, K.I., 2005. Shear-plate transducers as a possible alternative to bender elements for measuring G_{max}. Géotechnique 55 (5), 403–407. https://doi.org/10.1680/geot.2005.55.5.403

Itasca Consulting Group, 2007. PFC3D version 4.0 user manual, Minneapolis, MN, USA.

Ke, L., Takahashi, A., 2014. Experimental investigations on suffusion characteristics and its mechanical consequences on saturated cohesionless soil. Soils and Foundations 54 (4), 713–730. https://doi.org/10.1016/j.sandf.2014.06.024

Lade, P.V., Yamamuro, J.A., 1997. Effects of nonplastic fines on static liquefaction of sands. Canadian Geotechnical Journal 34 (6), 918–928. https://doi.org/10.1139/t97-052

Lawney, B.P., Luding, S., 2014. Frequency filtering in disordered granular chains. Acta Mechanica 225 (8), 2385–2407. https://doi.org/10.1007/s00707-014-1130-4

Magnanimo, V., La Ragione, L., Jenkins, J.T., Wang, P., Makse, H.A., 2008. Characterizing the shear and bulk moduli of an idealized granular material. Europhysics Letters 81 (3): 34006:1–6. https://doi.org/10.1209/0295-5075/81/34006

Makse, H.A., Gland, N., Johnson, D.L., Schwartz, L.M., 1999. Why effective medium theory fails in granular materials. Physical Review Letters 83 (24), 5070–5073. https://doi.org/10.1103/PhysRevLett.83.5070

Mitchell, J.K., 1976. Fundamentals of Soil Behaviour. *J. Wiley & Sons*, Toronto.

Mouraille, O., Luding, S., 2008. Sound wave propagation in weakly polydisperse granular materials. Ultrasonics 48 (6-7), 498–505. https://doi.org/10.1016/j.ultras.2008.03.009

Mouraille, O.J.P., 2009. Sound propagation in dry granular materials: discrete element simulations, theory, and experiments. University of Twente, Enschede, The Netherlands, Ph.D. thesis. https://doi.org/10.3990/1.9789036527897

Ni, Q., Tan, T.S., Dasari, G.R., Hight, D.W., 2004. Contribution of fines to the compressive strength of mixed soils. Géotechnique 54 (9), 561–569. https://doi.org/10.1680/geot.2004.54.9.561

O'Donovan, J., Ibraim, E., O'Sullivan, C., Hamlin, S., Muir Wood, D., Marketos, G., 2016. Micromechanics of seismic wave propagation in granular materials. Granular Matter 18 (56). https://doi.org/10.1007/s10035-015-0599-4

Otsubo, M., 2016. Particle scale analysis of soil stiffness and elastic wave propagation. Imperial College London, London, UK, Ph.D. thesis.

Otsubo, M., O'Sullivan, C., Hanley, K.J., Sim, W., 2017a. Influence of packing density and stress on the dynamic response of granular materials. Granular Matter 19 (50), 1-18. https://doi.org/10.1007/s10035-017-0729-2

Otsubo, M., O'Sullivan, C., Hanley, K.J., Sim, W., 2017b. The influence of particle surface roughness on elastic stiffness and dynamic response. Géotechnique 67 (5), 452–459. https://doi.org/10.1680/jgeot.16.P.050

Otsubo, M., O'Sullivan, C., 2018. Experimental and DEM assessment of the stress-dependency of surface roughness effects on shear modulus. Soils and Foundations 58 (3), 602–614. https://doi.org/10.1016/j.sandf.2018.02.020

Otsubo, M., Dutta, T.T., Durgalian, M., Kuwano, R., O'Sullivan, C., 2019. Particle-scale insight into transitional behaviour of gap-graded materials – small-strain stiffness and frequency response. E3S Web of Conferences, 92, *7th International Symposium on Deformation Characteristics of Geomaterials (IS-Glasgow 2019)*, 14006. https://doi.org/10.1051/e3sconf/20199214006

Plimpton, S., 1995. Fast parallel algorithms for short-range molecular dynamics. Journal of Computational Physics 117 (1), 1–19. https://doi.org/10.1006/jcph.1995.1039

Rahman, M.M., Lo, S.R., Gnanendran, C.T., 2008. On equivalent granular void ratio and steady state behaviour of loose sand with fines. Canadian Geotechnical Journal 45 (10), 1439–1456. https://doi.org/10.1139/T08-064

Salgado, R., Bandini, P., Karim, A., 2000. Shear strength and stiffness of silty sand. Journal of Geotechnical and Geoenvironmental Engineering 126 (5), 451–462. https://doi.org/10.1061/(ASCE)1090-0241(2000)126:5(451)

Santamarina, J.C., Klein, K.A., Fam, M.A., 2001. Soils and waves: Particulate materials behavior, characterization and process monitoring, *Wiley*, Hoboken, New Jersey. ISBN: 978-0-471-49058-6

Sato, M., Kuwano, R., 2015. Suffusion and clogging by one-dimensional seepage tests on cohesive soil, Soils and Foundations 55 (6), 1427–1440. https://doi.org/10.1016/j.sandf.2015.10.008

Shirley, D.J., Hampton, L.D., 1978. Shear-wave measurements in laboratory sediments. The Journal of the Acoustical Society of America 63 (2), 607–613. https://doi.org/10.1121/1.381760

Shire, T., O'Sullivan, C., Hanley, K.J., Fannin, R.J., 2014. Fabric and effective stress distribution in internally unstable soils. Journal of Geotechnical and Geoenvironmental Engineering 140 (12). https://doi.org/10.1061/(ASCE)GT.1943-5606.0001184

Shire, T., O'Sullivan, C., Hanley, K.J., 2016. The influence of fines content and size-ratio on the micro-scale properties of dense bimodal materials, Granular Matter 18 (52), 1-10. https://doi.org/10.1007/s10035-016-0654-9

Skempton, A.W., Brogan, J.M., 1994. Experiments on piping in sandy gravels. Géotechnique 44 (3), 449–460. https://doi.org/10.1680/geot.1994.44.3.449

Suwal, L.P., Kuwano, R., 2013. Disk shaped piezo-ceramic transducer for P and S wave measurement in a laboratory soil specimen, Soils and Foundations 53 (4), 510–524. https://doi.org/10.1016/j.sandf.2013.06.004

The Japanese Geotechnical Society, 2009. Test method for minimum and maximum densities of sands, JGS 0161:2009 (JIS A 1224:2009). Japanese Geotechnical Society.

Thevanayagam, S., 1998. Effect of fines and confining stress on undrained shear strength of silty sands. Journal of Geotechnical and Geoenvironmental Engineering 124 (6), 479–491. https://doi.org/10.1061/(ASCE)1090-0241(1998)124:6(479)

Thevanayagam, S., Shenthan, T., Mohan, S., Liang, J., 2002. Undrained fragility of clean sands, silty sands, and sandy silts. Journal of Geotechnical and Geoenvironmental Engineering 128 (10), 849–859. https://doi.org/10.1061/(ASCE)1090-0241(2002)128:10(849)

Thornton, C., 2000. Numerical simulations of deviatoric shear deformation of granular media. Géotechnique 50 (1), 43–53. https://doi.org/10.1680/geot.2000.50.1.43

Yamashita, S., Kawaguchi. T., Nakata, Y. Mikami, T., Fujiwara, T. Shibuya, S., 2009. Interpretation of international parallel test on the measurement of G_{max} using bender elements. Soils and Foundations 49 (4), 631–650. https://doi.org/10.3208/sandf.49.631

Yang, J., Liu, X., 2016. Shear wave velocity and stiffness of sand: the role of non-plastic fine. Géotechnique 66 (6), 500–514. https://doi.org/10.1680/jgeot.15.P.205

Yimsiri, S., Soga, K., 2000. Micromechanics-based stress–strain behaviour of soils at small strains. Géotechnique 50 (5), 559–571. https://doi.org/10.1680/geot.2000.50.5.559

Zuo, L., Baudet, B.A., 2015. Determination of the transitional fines content of sand-non plastic fines mixtures. Soils and Foundations 55 (1), 213–219. https://doi.org/10.1016/j.sandf.2014.12.017

Table 1 Summary of samples considered.

Material	Size of coarse particles (D)	Size of finer particles (d)	$R_d = D_{50}/d_{50}$	D_{15}/d_{85}	D_{10}/d_{50}
	mm	mm			
Narrowly gap-graded (GN)	1.2 – 2.2	0.4 – 0.65	3.4	2.6	2.7
Widely gap-graded (GW)		0.15 – 0.25	8.8	6.7	6.9

Table 2 GN samples for DEM simulations at p'=100 kPa.

Sample	Number of particles	Density	F_C (actual)	L	W	e	$\overline{C_N}$	e^{mech}	α^{ff}	V_S	f_{lp}
				m	m					m/s	kHz
1	13,632	Dense	0.0	0.148	0.022	0.555	5.58	0.611	0.0	352	27.5
2		Medium		0.150	0.022	0.615	4.97	0.690	0.0	310	18.2
3		Loose		0.151	0.022	0.655	4.32	0.786	0.0	256	10.8
4	71,400	Dense	0.1 (0.097)	0.153	0.022	0.448	1.63	0.603	0.03	351	27.8
5		Medium		0.154	0.022	0.493	1.31	0.684	0.03	311	20.4
6		Loose		0.155	0.023	0.527	1.09	0.779	0.02	251	10.8
7	126,797	Dense	0.20 (0.192)	0.149	0.022	0.372	2.64	0.548	0.23	370	37.4
8		Medium		0.151	0.022	0.409	1.48	0.674	0.16	304	21.3
9		Loose		0.151	0.022	0.442	0.91	0.797	0.10	235	11.3
10	174,657	Dense	0.25 (0.230)	0.157	0.023	0.363	3.82	0.482	0.37	386	42.5
11		Medium		0.158	0.023	0.389	2.25	0.618	0.29	314	25.8
12		Loose		0.159	0.023	0.414	1.13	0.772	0.17	230	11.2
13	199,800	Dense	0.3 (0.293)	0.157	0.022	0.365	4.79	0.438	0.57	401	54.6
14		Medium		0.158	0.022	0.390	3.61	0.533	0.50	337	31.7
15		Loose		0.159	0.022	0.409	1.78	0.743	0.31	240	14.1
16	250,516	Dense	0.35 (0.343)	0.157	0.023	0.373	5.10	0.432	0.67	404	57.3
17		Medium		0.159	0.023	0.400	4.19	0.504	0.63	348	38.7
18		Loose		0.159	0.023	0.419	2.54	0.688	0.44	255	16.4
19	241,123	Dense	0.4 (0.393)	0.149	0.022	0.383	5.28	0.435	0.73	404	58.7
20		Medium		0.151	0.022	0.414	4.72	0.476	0.71	346	42.6
21		Loose		0.151	0.022	0.437	3.08	0.651	0.54	266	20.5
22	341,372	Dense	0.6 (0.593)	0.149	0.022	0.434	5.70	0.463	0.90	387	61.3
23		Medium		0.151	0.022	0.474	4.89	0.538	0.89	341	46.4
24		Loose		0.152	0.022	0.503	3.98	0.643	0.82	274	26.7
25	432,696	Dense	0.8 (0.797)	0.149	0.022	0.495	5.85	0.512	0.97	371	65.5
26		Medium		0.151	0.022	0.542	5.08	0.594	0.97	328	48.9
27		Loose		0.152	0.022	0.577	4.28	0.699	0.94	268	29.8
28	497,961	Dense	1.0	0.147	0.022	0.558	5.87	0.576	1.0	354	76.9
29		Medium		0.149	0.022	0.613	5.18	0.656	1.0	314	54.2
30		Loose		0.150	0.022	0.652	4.49	0.755	1.0	258	31.5

Table 3 GW samples for DEM simulations at p'=100 kPa.

Sample	Number of particles	Density	F_C (actual)	L	W	e	$\overline{C_N}$	e^{mech}	α^{ff}	V_S	f_{lp}
				m	m					m/s	kHz
31	965,420	Dense	0.1 (0.100)	0.138	0.022	0.414	0.08	0.608	0.00	351	27.3
32		Medium		0.140	0.022	0.461	0.07	0.691	0.00	311	19.5
33		Loose		0.141	0.022	0.495	0.06	0.789	0.00	256	10.7
34	1,870,173	Dense	0.20 (0.200)	0.140	0.02	0.256	0.04	0.607	0.00	353	27.8
35		Medium		0.141	0.021	0.301	0.03	0.696	0.00	308	18.8
36		Loose		0.142	0.021	0.336	0.03	0.826	0.00	240	9.7
37	1,993,622	Dense	0.25 (0.249)	0.140	0.019	0.216	5.43	0.234	0.29	471	50.3
38		Medium		0.140	0.019	0.230	0.50	0.652	0.00	300	16.8
39		Loose		0.141	0.019	0.271	0.03	0.863	0.00	215	8.0
40	1,873,508	Dense	0.3 (0.300)	0.139	0.017	0.237	5.65	0.250	0.85	497	94.5
41		Medium		0.139	0.017	0.254	4.75	0.288	0.69	433	68.1
42		Loose		0.139	0.017	0.247	0.03	0.929	0.00	152	4.7
43	2,286,346	Dense	0.35 (0.350)	0.137	0.017	0.259	5.60	0.278	0.98	481	92.6
44		Medium		0.137	0.017	0.279	4.87	0.312	0.88	425	70.4
45		Loose		0.138	0.017	0.293	3.86	0.369	0.45	327	34.7
46	1,011,169	Dense	0.4 (0.402)	0.136	0.011	0.282	5.62	0.303	1.02	467	88.0
47		Medium		0.137	0.011	0.305	4.86	0.343	0.96	412	75.5
48		Loose		0.137	0.011	0.323	4.04	0.395	0.74	333	41.7
49	1,439,829	Dense	0.6 (0.596)	0.130	0.011	0.370	5.78	0.388	1.05	419	75.7
50		Medium		0.131	0.011	0.402	5.01	0.445	1.03	370	62.6
51		Loose		0.132	0.011	0.428	4.22	0.515	0.97	304	47.8
52	1,493,179	Dense	0.8 (0.793)	0.128	0.010	0.460	5.88	0.473	1.03	381	75.7
53		Medium		0.130	0.010	0.502	5.16	0.537	1.03	337	63.6
54		Loose		0.131	0.010	0.534	4.42	0.623	1.01	279	50.8
55	248,249	Dense	1.0	0.151	0.004	0.557	5.76	0.593	1.00	356	179.9
56		Medium		0.153	0.004	0.609	5.09	0.670	1.00	316	115.1
57		Loose		0.154	0.004	0.642	4.52	0.770	1.00	282	74.1

Table 4 Summary of range of threshold fines contents (F_{thre}) at p'=100 kPa, determined using different available approaches.

Material type	Density	e	e^{mech}	$\overline{C_N}$	α^{ff}	α	V_s	f_{lp}
GN	Dense	25–30%	10–20%	10–20%	10–20%	0–10%	10–20%	10–20%
	Medium	25–30%	20–25%	20–25%	10–20%	0–10%	20–25%	20–25%
	Loose	30–35%	20–25%	25–30%	10–20%	0–10%	25–30%	25–30%
GW	Dense	25–30%	20–25%	20–25%	20–25%	20–25%	20–25%	20–25%
	Medium	25–30%	25–30%	25–30%	25–30%	25–30%	25–30%	25–30%
	Loose	30–35%	30–35%	30–35%	30–35%	30–35%	30–35%	30–35%

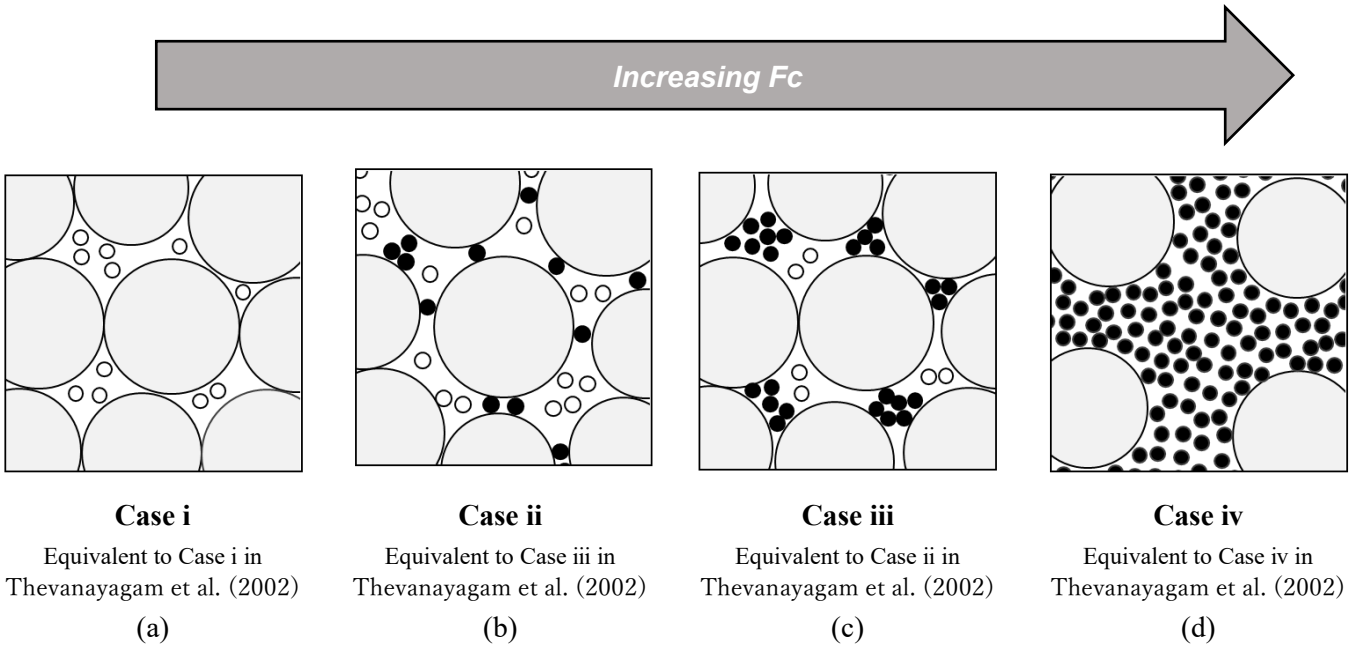

Figure 1 Schematic diagrams of gap-graded fabric (a) underfilled fabric (b) transitional fabric with a loose packing (c) transitional fabric with a dense packing (d) overfilled fabric. (The color of finer particles indicates whether the finer particle is loaded (back) or not loaded (white)).

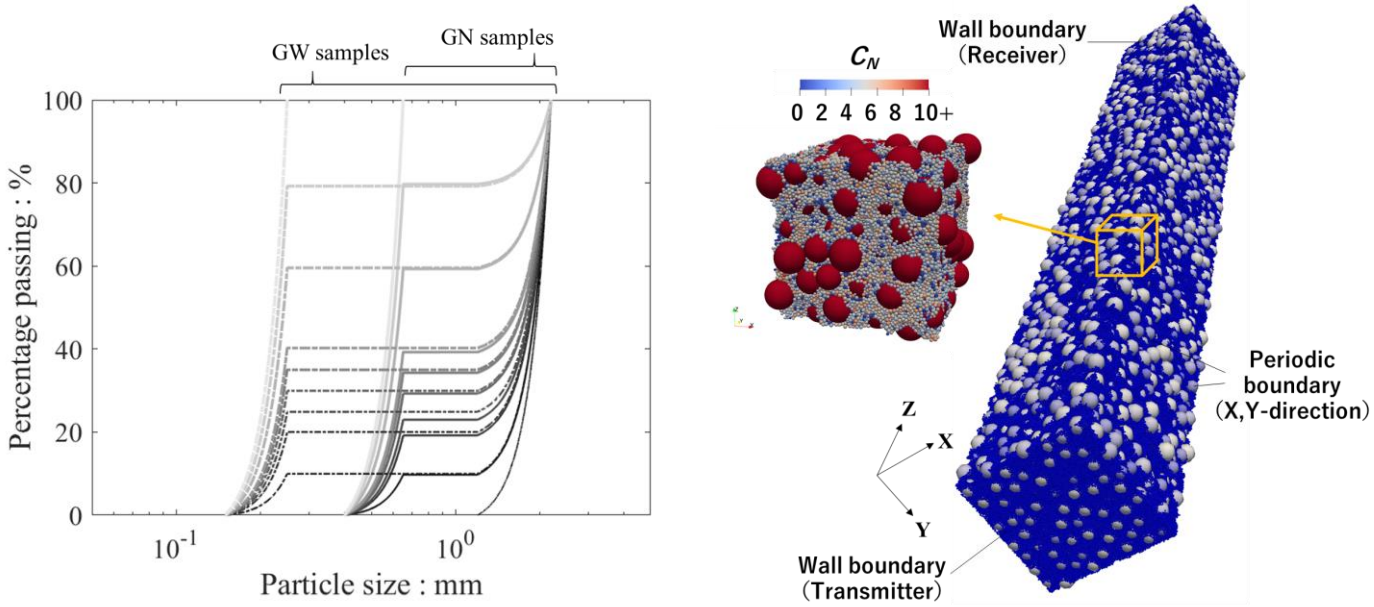

(a) (b)

Figure 2 (a) Particle size distribution of tested samples (b) medium dense GW sample with F_C=20% illustrated with boundary conditions. *C_N is the number of contacts the particle participates in.*

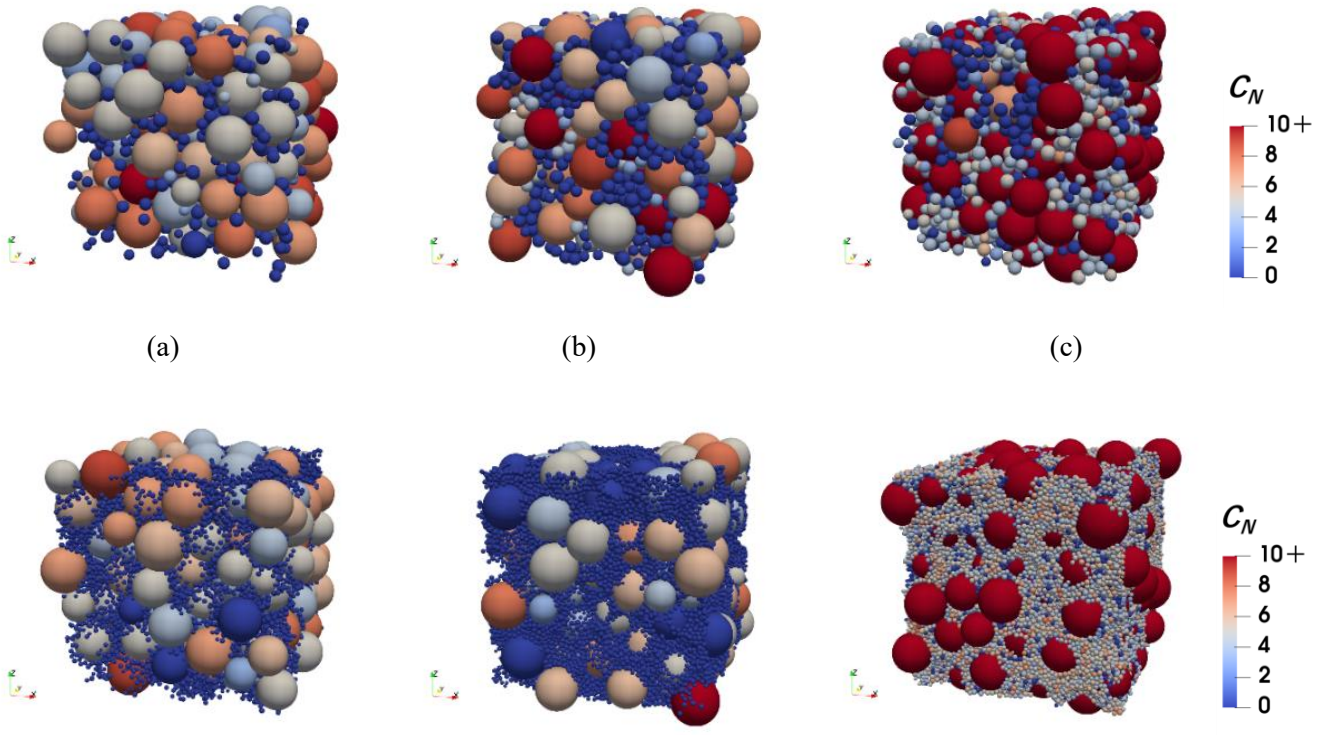

Figure 3 Representative core of medium dense samples (10×10×10 mm) with differing F_C values at p'=100 kPa (a) GN, F_C=10% (b) GN, F_C=20% (c) GN, F_C=30% (d) GW, F_C=10% (e) GW, F_C=20% (f) GW, F_C=30%. *C_N is the number of contacts the particle participates in.*

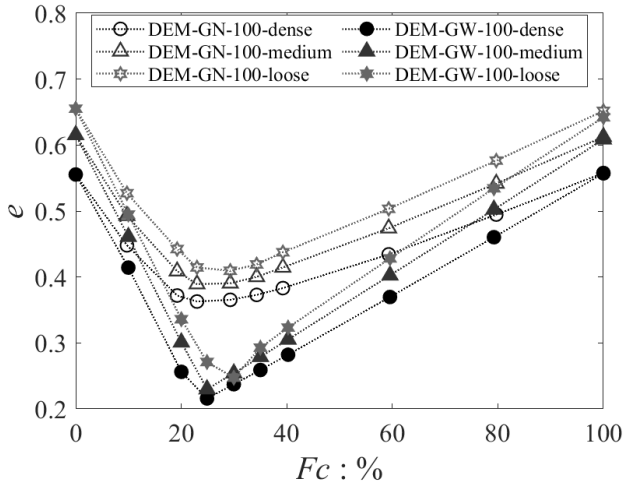

(a)

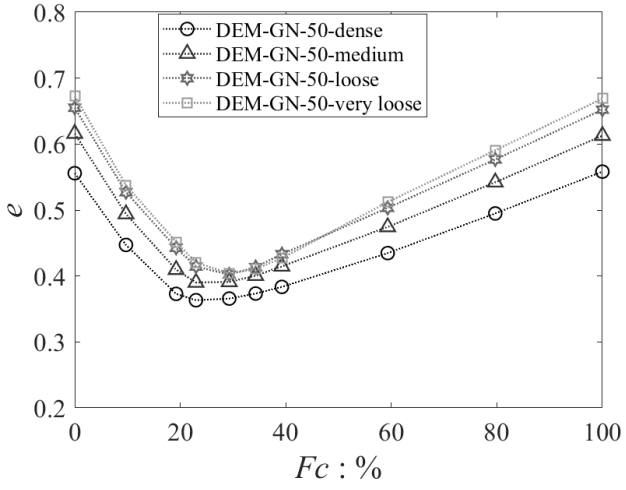

(b)

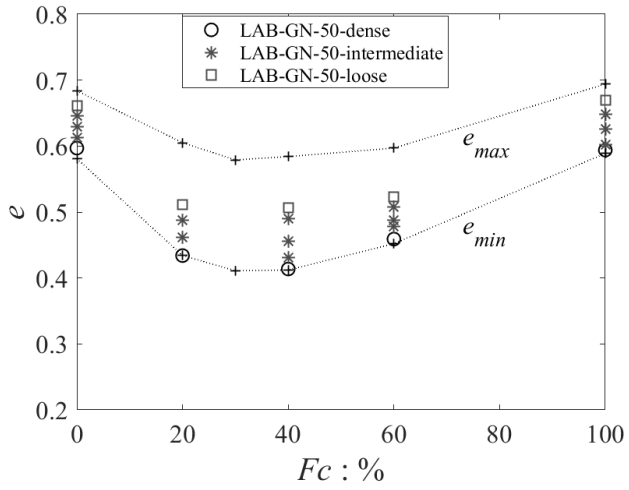

(c)

Figure 4 Variations in void ratio with F_C (a) DEM data for GN and GW samples at p'=100 kPa (b) DEM data for GN samples at p'=50 kPa (c) experimental data for GN samples at p'=50 kPa.

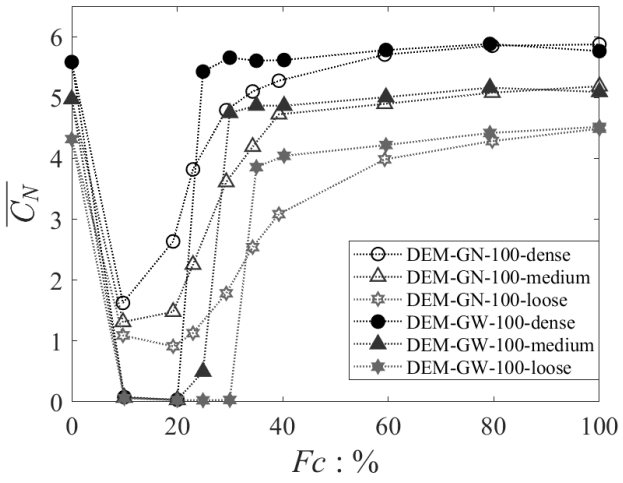

(a)

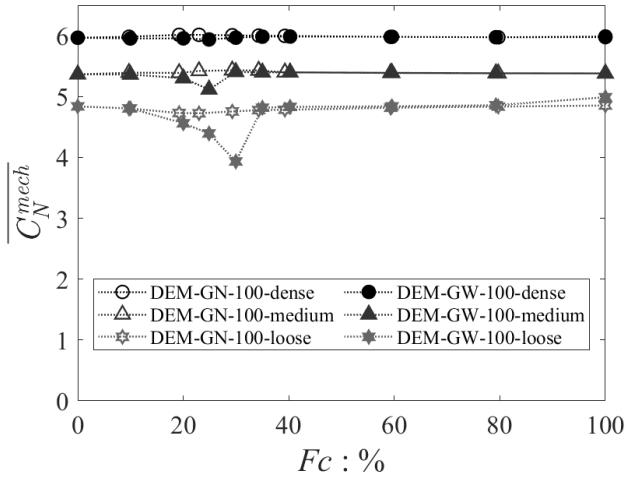

(b)

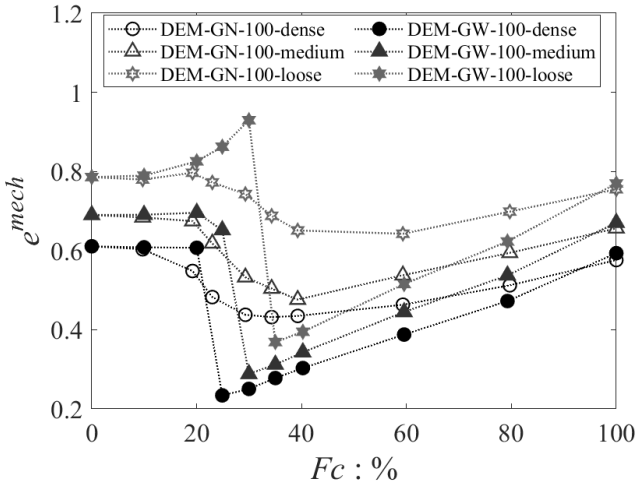

(c)

Figure 5 Variations in (a) mean coordination number (b) mean mechanical coordination number and (c) mechanical void ratio, with fines content F_C for DEM samples at p'=100 kPa.

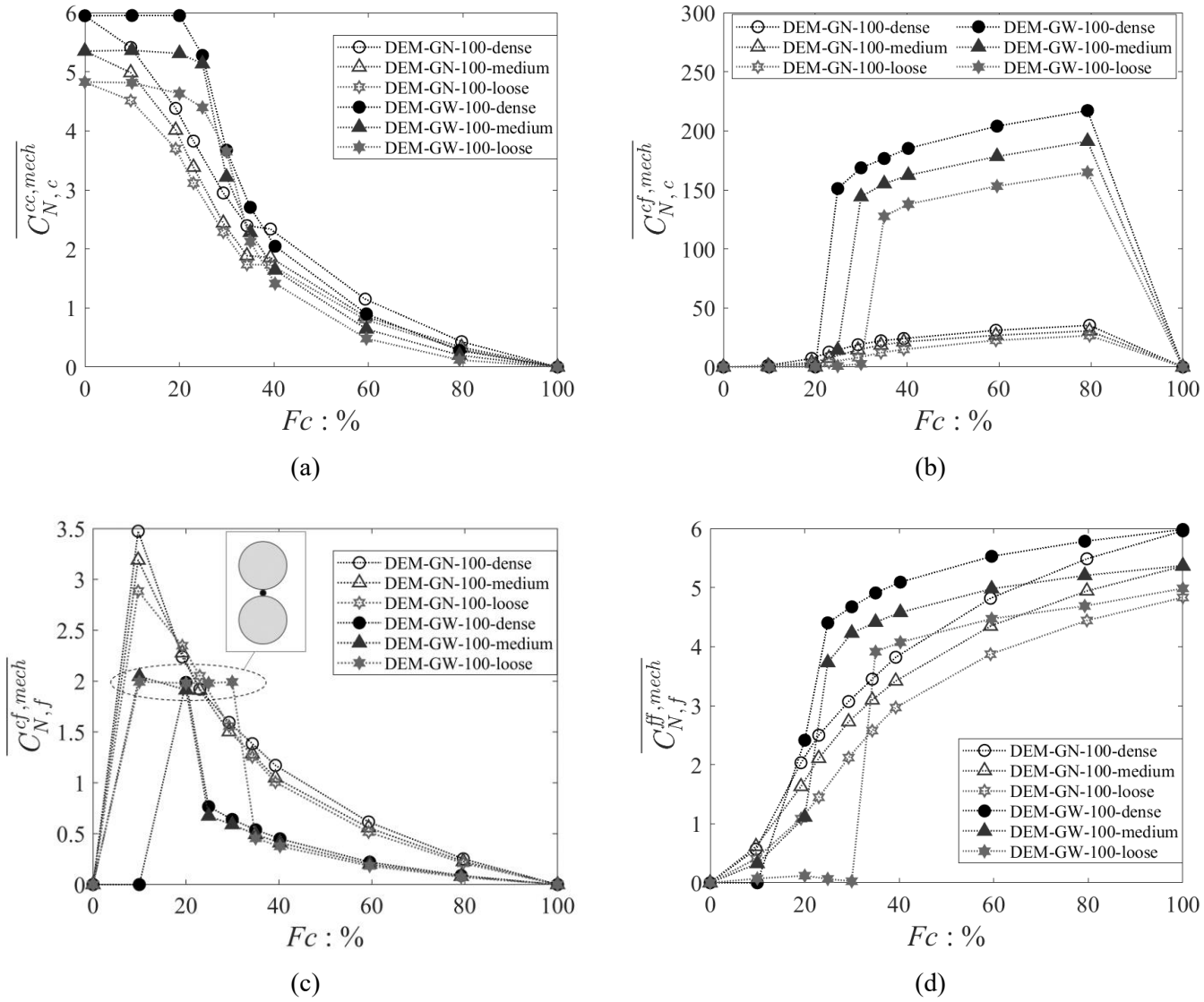

Figure 6 Mean mechanical coordination number for DEM samples at p'=100 kPa (a) coarse-coarse particle contacts per coarse particle (b) coarse-finer particle contacts per coarse particle (c) coarse-finer particle contacts per finer particle (d) finer-finer particle contacts per finer particle.

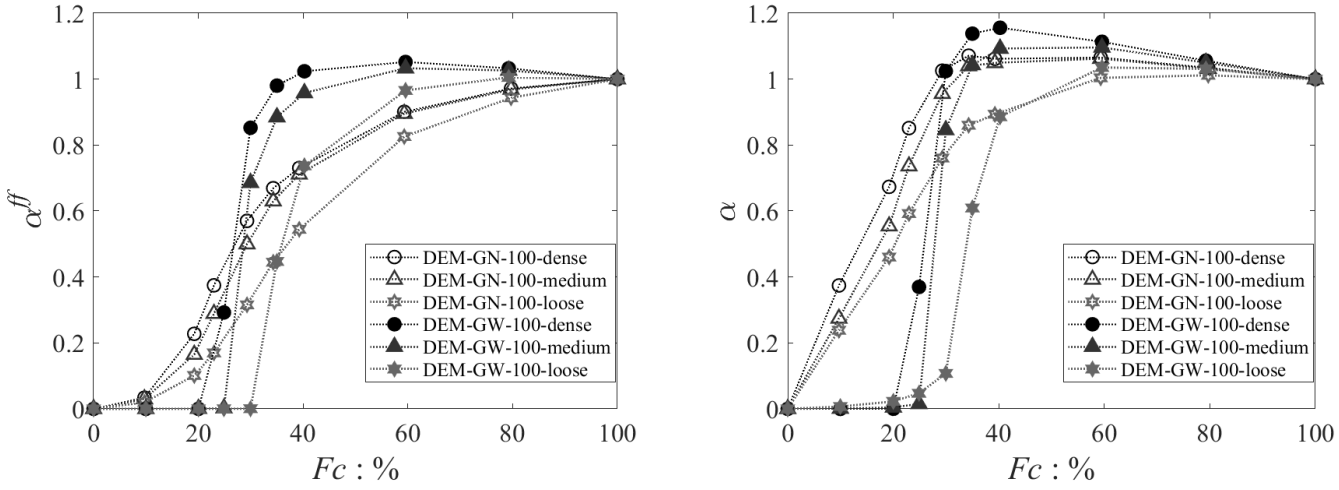

(a) (b)

Figure 7 Inhomogeneity of stress transfer in DEM samples at p'=100 kPa (a) finer-finer particle contacts only (b) finer particles (i.e. finer-finer and finer-coarse particle contacts) following Shire et al. (2014).

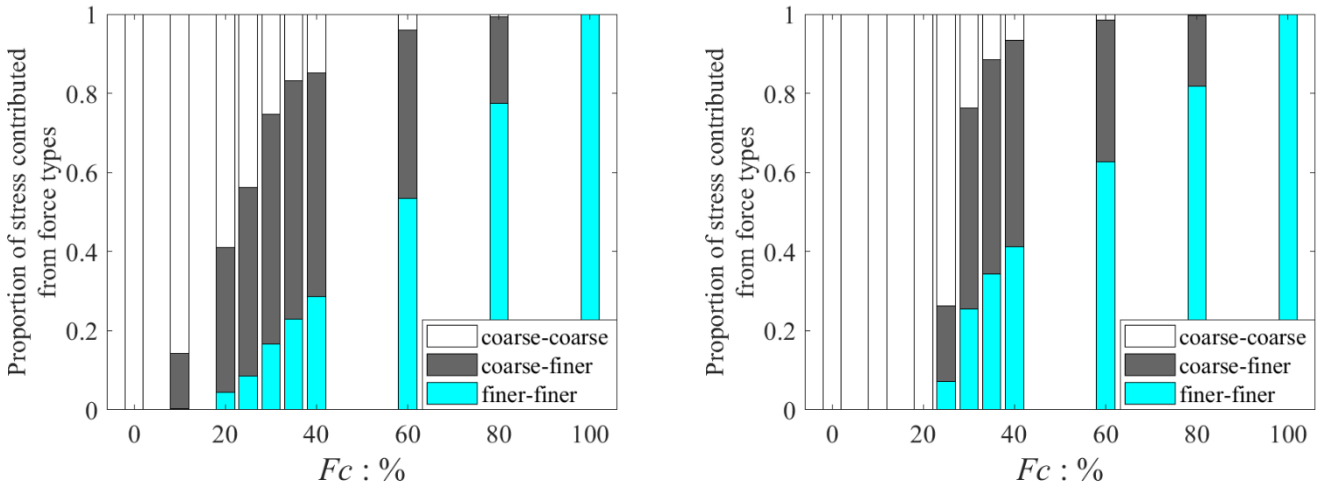

(a) (b)

Figure 8 Contribution to overall stress tensor from different contact types, i.e. coarse-coarse, coarse-finer and finer-finer particle contacts, for DEM data at p'=100 kPa (a) Dense GN samples (b) Dense GW samples.

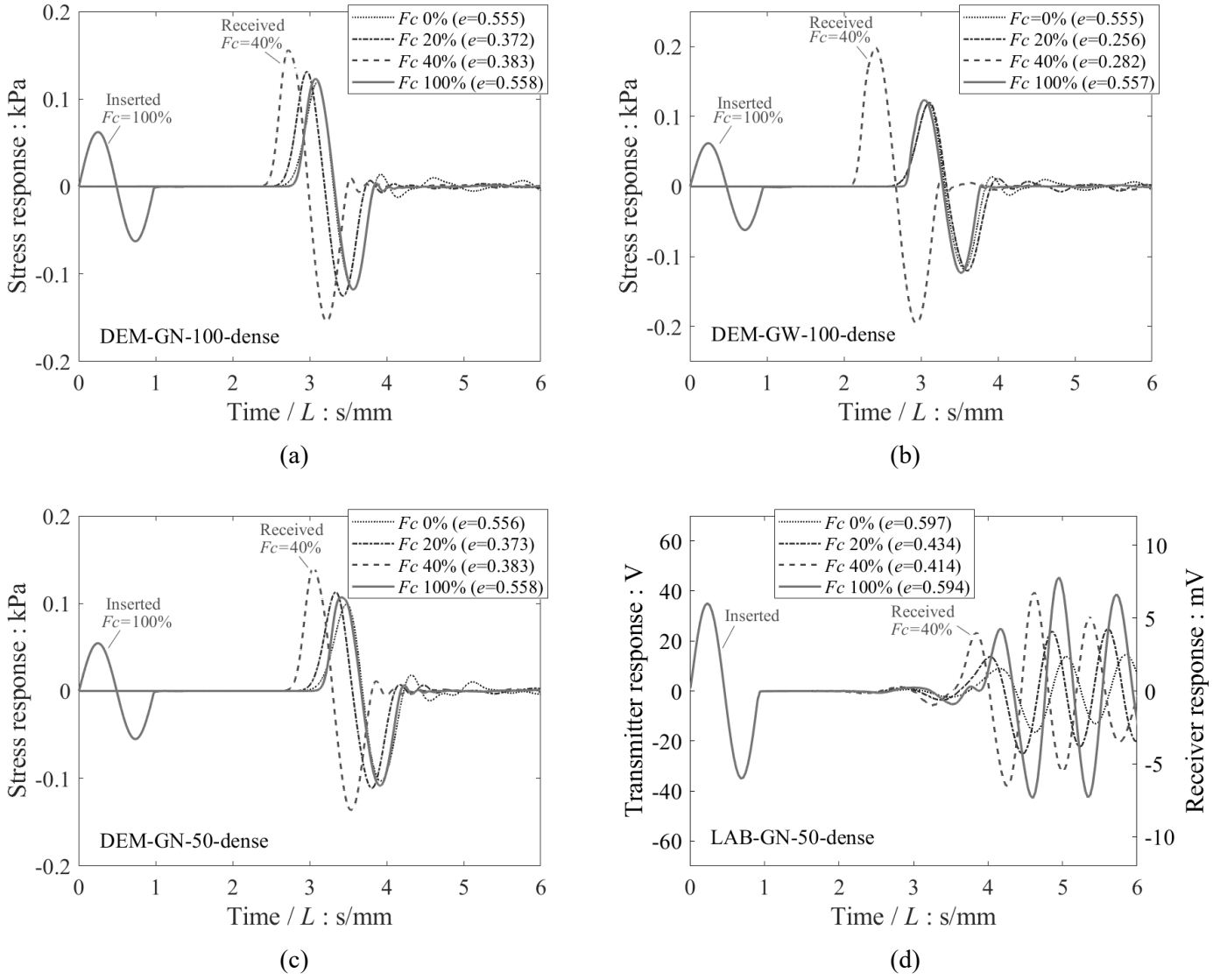

Figure 9 Time domain responses for shear wave propagation in dense samples with f_{in}=7 kHz for F_C=0%, 20%, 40% and 100% (a) DEM data for GN dense samples at p'=100 kPa (b) DEM data for GW dense samples at p'=100 kPa (c) DEM data for GN dense samples at p'=50 kPa (d) experimental data for GN dense samples at p'=50 kPa.

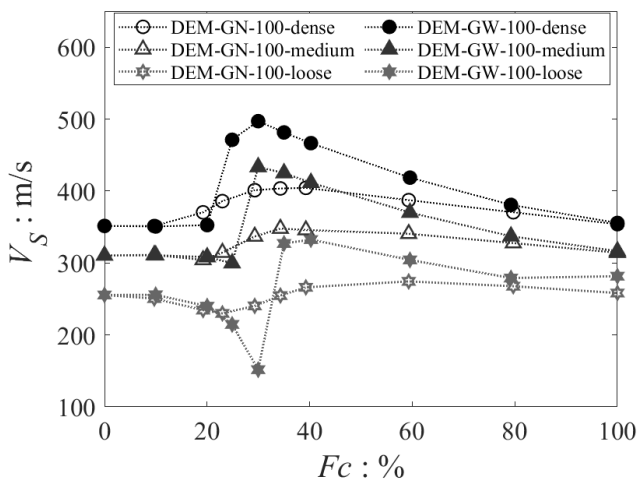

(a)

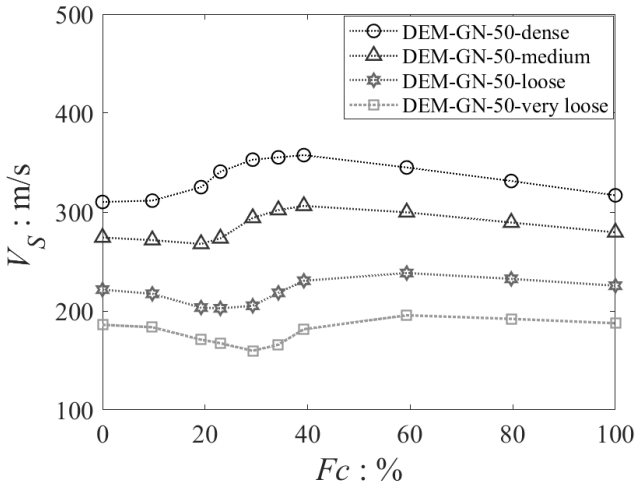

(b)

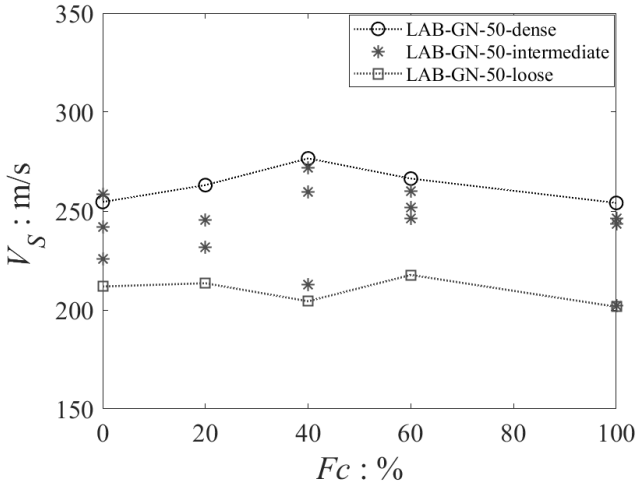

(c)

Figure 10 Variations in V_S with F_C determined from stress wave propagation (a) DEM data for GN and GW samples at p'=100 kPa (b) DEM data for GN samples at p'=50 kPa (c) experimental data for GN samples at p'=50 kPa.

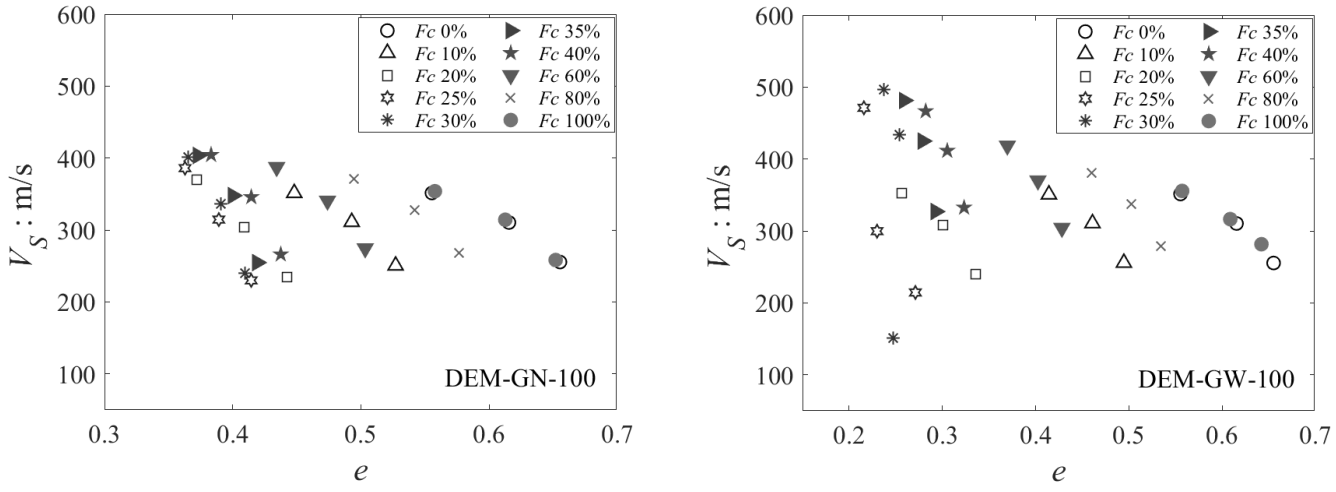

(a) (b)

Figure 11 Relationship between V_S and global void ratio for DEM simulations at p'=100 kPa (a) GN samples (b) GW samples.

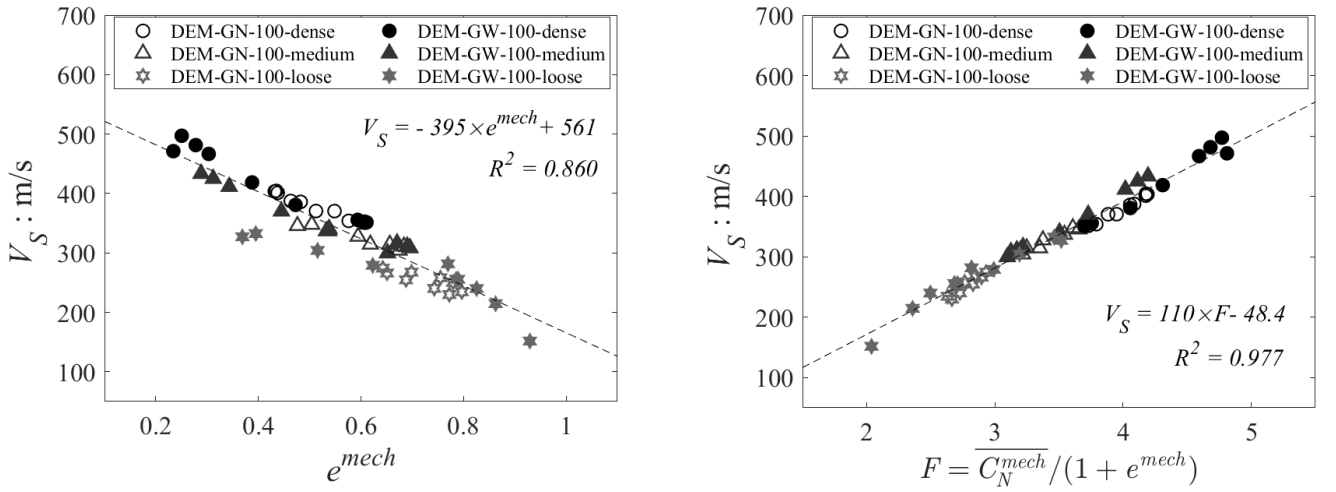

(a) (b)

Figure 12 Correlation between V_S and packing properties for DEM simulation data (a) mechanical void ratio (b) a function considering both mechanical void ratio and mean mechanical coordination number.

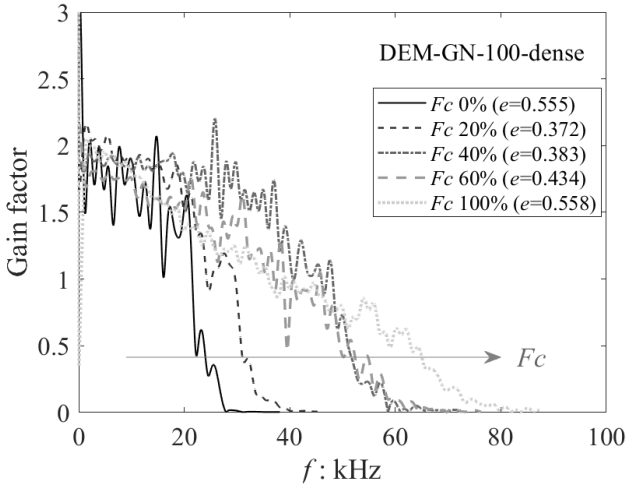

(a)

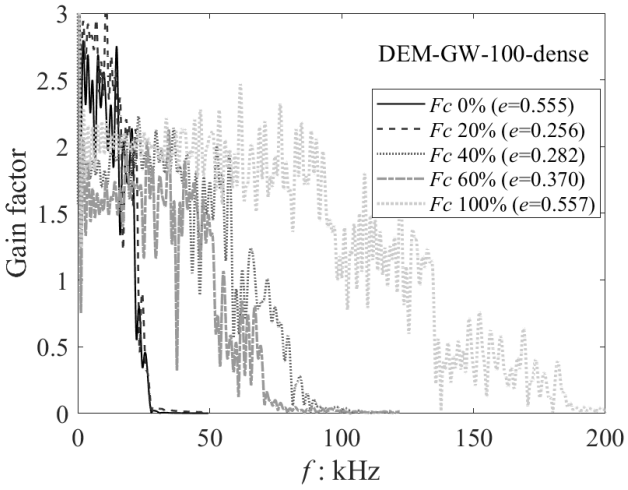

(b)

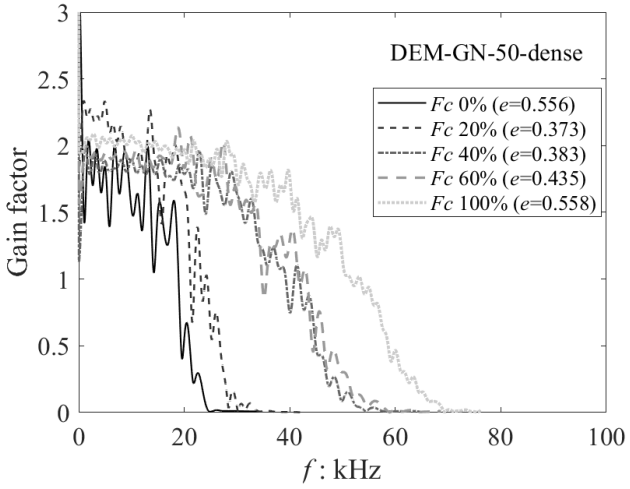

(c)

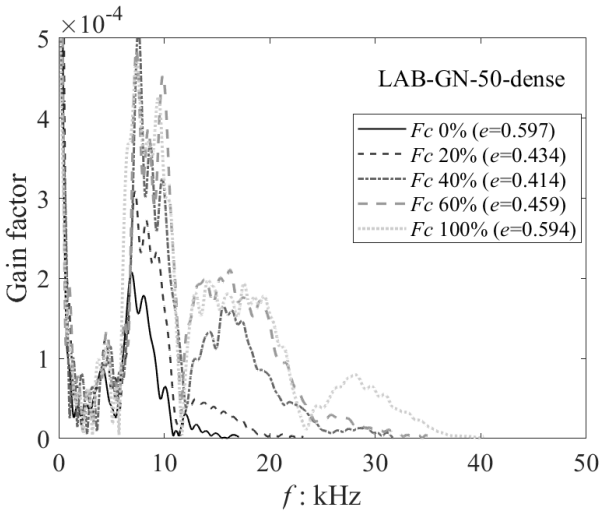

(d)

Figure 13 Frequency domain responses for shear wave propagation in dense samples for F_C=0%, 20%, 40% and 100% (a) DEM data for GN dense samples at p'=100 kPa (b) DEM data for GW dense samples at p'=100 kPa (c) DEM data for GN dense samples at p'=50 kPa (d) experimental data for GN dense samples at p'=50 kPa.

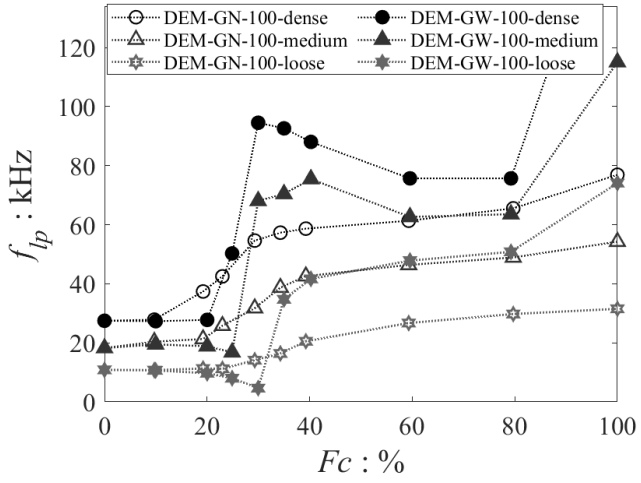

(a)

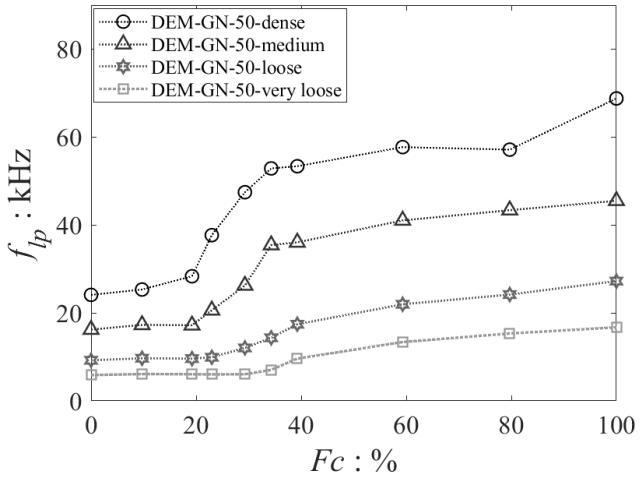

(b)

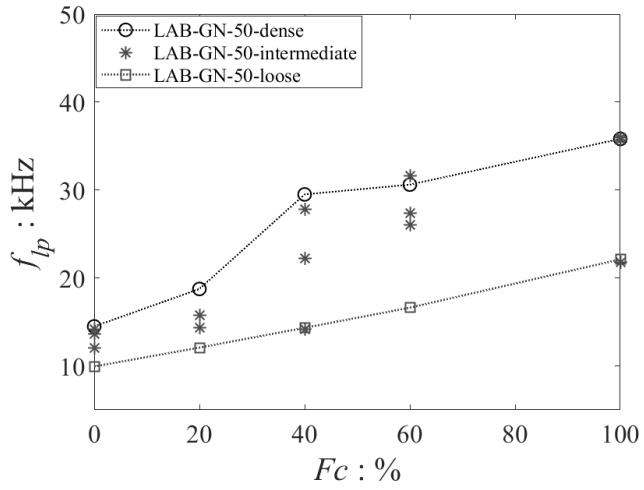

(c)

Figure 14 Variation in lowpass frequency f_{lp} with Fc, determined from stress wave propagation (a) DEM data for GN and GW samples at p'=100 kPa (b) DEM data for GN samples at p'=50 kPa (c) experimental data for GN samples at p'=50 kPa.

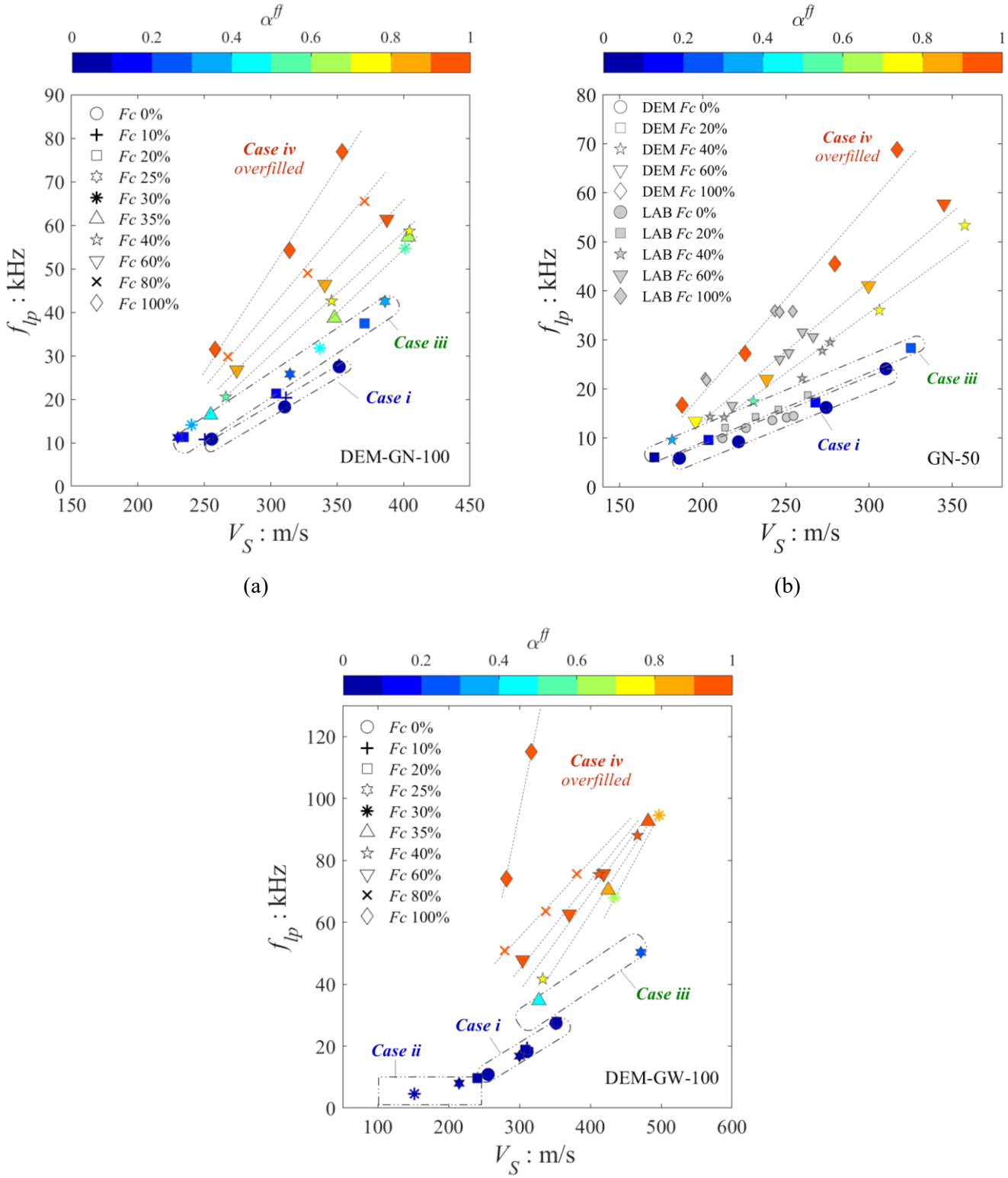

Figure 15 Relationship between f_{lp} and V_S for (a) DEM GW samples at p'=100 kPa, coloured by α^{ff} value (b) Combined DEM and experimental data for GN samples at p'=50 kPa (DEM data are coloured by α^{ff} value) (c) DEM GN samples at p'=100 kPa, coloured by α^{ff} value.